

This is an Accepted Manuscript of the following article:

Peter E. Land, Helen S. Findlay, Jamie D. Shutler, Ian G.C. Ashton, Thomas Holding, Antoine Grouazel, Fanny Girard-Ardhuin, Nicolas Reul, Jean-Francois Piolle, Bertrand Chapron, Yves Quilfen, Richard G.J. Bellerby, Punyasloke Bhadury, Joseph Salisbury, Douglas Vandemark, Roberto Sabia. Optimum satellite remote sensing of the marine carbonate system using empirical algorithms in the global ocean, the Greater Caribbean, the Amazon Plume and the Bay of Bengal. *Remote Sensing of Environment*. 235, 2019, 111469, ISSN 1879-0704.

The article has been published in final form by Elsevier at

<https://doi.org/10.1016/j.rse.2019.111469>

© 2019. This manuscript version is made available under the

CC-BY-NC-ND 4.0 license

<http://creativecommons.org/licenses/by-nc-nd/4.0/>

---

1 **Optimum satellite remote sensing of the marine carbonate system using empirical**  
2 **algorithms in the Global Ocean, the Greater Caribbean, the Amazon Plume and the**  
3 **Bay of Bengal**

4

5 Peter E. Land and Helen S. Findlay, Plymouth Marine Laboratory, Prospect Place, West Hoe,  
6 Plymouth, PL1 3DH, UK

7 Jamie D. Shutler, Ian G.C. Ashton and Thomas Holding, University of Exeter, Penryn,  
8 Cornwall, TR10 9FE, UK

9 Antoine Grouazel, Fanny Girard-Ardhuin, Nicolas Reul, Jean-Francois Piolle, Bertrand  
10 Chapron and Yves Quilfen, Ifremer, University Brest, CNRS, IRD, Laboratoire  
11 d'Océanographie Physique et Spatiale (LOPS), IUEM, F-29280, Brest, France.

12 Richard G.J. Bellerby, SKLEC-NIVA Centre for Marine and Coastal Research, State Key  
13 Laboratory for Estuarine and Coastal Research, East China Normal University Zhongshan N.  
14 Road, 3663, Shanghai 200062, China; and Norwegian Institute for Water Research,  
15 Thormøensgate 53D, N-5006, Bergen, Norway.

16 Punyasloke Bhadury, Department of Biological Sciences, Indian Institute of Science  
17 Education and Research Kolkata, Mohanpur 741 246, West Bengal, India

18 Joseph Salisbury and Douglas Vandemark, Ocean Processes Analysis Laboratory, University  
19 of New Hampshire, Durham, New Hampshire, 3824, United States

20 Roberto Sabia, Telespazio-Vega U.K. for European Space Agency (ESA), ESRIN, Frascati,  
21 Italy

22

23 Corresponding author: P. E. Land, Plymouth Marine Laboratory, Prospect Place, West Hoe,  
24 Plymouth, PL1 3DH, UK. ([peland@pml.ac.uk](mailto:peland@pml.ac.uk))

25

26 Research highlights

- 27 • Satellite salinity measurements enable estimation of surface carbonate parameters.
- 28 • Uncertainties within these observation-based estimates are well characterized.
- 29 • Monthly satellite salinity and temperature allows synoptic monitoring.
- 30 • Satellite observations allow study of seasonal, interannual and episodic variations

31

32 **Abstract**

33 Improving our ability to monitor ocean carbonate chemistry has become a priority as the  
34 ocean continues to absorb carbon dioxide from the atmosphere. This long-term uptake is  
35 reducing the ocean pH; a process commonly known as ocean acidification. The use of  
36 satellite Earth Observation has not yet been thoroughly explored as an option for routinely  
37 observing surface ocean carbonate chemistry, although its potential has been highlighted. We  
38 demonstrate the suitability of using empirical algorithms to calculate total alkalinity ( $A_T$ ) and  
39 total dissolved inorganic carbon ( $C_T$ ), assessing the relative performance of satellite,  
40 interpolated *in situ*, and climatology datasets in reproducing the wider spatial patterns of  
41 these two variables. Both  $A_T$  and  $C_T$  *in situ* data are reproducible, both regionally and  
42 globally, using salinity and temperature datasets, with satellite observed salinity from  
43 Aquarius and SMOS providing performance comparable to other datasets for the majority of  
44 case studies. Global root mean squared difference (RMSD) between *in situ* validation data  
45 and satellite estimates is  $17 \mu\text{mol kg}^{-1}$  with bias  $< 5 \mu\text{mol kg}^{-1}$  for  $A_T$  and  $30 \mu\text{mol kg}^{-1}$  with  
46 bias  $< 10 \mu\text{mol kg}^{-1}$  for  $C_T$ . This analysis demonstrates that satellite sensors provide a  
47 credible solution for monitoring surface synoptic scale  $A_T$  and  $C_T$ . It also enables the first  
48 demonstration of observation-based synoptic scale  $A_T$  and  $C_T$  temporal mixing in the  
49 Amazon plume for 2010-2016, complete with a robust estimation of their uncertainty.

50

51

52 **Keywords**

53 Carbonate chemistry; Earth observation; Ocean acidification; Total alkalinity; Dissolved  
54 inorganic carbon; SMOS; Aquarius; CORA; HadGEM2-ES

## 55 1. Introduction

56 The oceans play an important role in absorbing carbon (e.g. Sabine et al., 2004), and the  
57 increase in CO<sub>2</sub> emitted into the atmosphere as a result of anthropogenic activities has  
58 resulted in an increase in CO<sub>2</sub> uptake by the oceans (Caldeira and Wickett, 2005; Sabine et  
59 al., 2004; Takahashi et al., 2009). This long-term absorption results in a shift in ocean  
60 carbonate chemistry, which has the potential to alter biogeochemical cycles and ecosystem  
61 function in the future (Raven et al., 2005; Kroeker et al. 2013). As a result of the decrease in  
62 ocean pH arising from these shifts (often termed Ocean Acidification), this change in ocean  
63 carbonate chemistry has received increasing scientific and political attention over the past  
64 decade. This has led to questions about the magnitude and importance of spatial and temporal  
65 ocean carbon variability, as well as how to monitor ongoing change at global and regional  
66 scales. To-date, carbonate system monitoring has been primarily from ship- and field-based  
67 observations that provide relatively disparate and sparse datasets of carbonate chemistry  
68 parameters in both space and time. To expand capabilities, state-of-the-art autonomous *in situ*  
69 tools are needed (Byrne, 2014). Recent advances include pH sensors on biogeochemical  
70 floats (e.g. Johnson *et al.*, 2017), and sensors to observe multiple carbonate system  
71 parameters *in situ* are now in development (Bushinsky *et al.*, 2019). One such advancement is  
72 utilizing Earth Observation (EO) satellites to provide wider spatial and temporal coverage of  
73 surface carbonate chemistry observations, with the aim of detecting features and  
74 characterizing dynamics that are difficult to resolve using *in situ* datasets (Land *et al.*, 2015;  
75 Salisbury *et al.*, 2015; Fine *et al.*, 2017). Currently, there are just two satellites in orbit that  
76 are specifically designed to support global carbon cycle research (The US NASA Orbiting  
77 Carbon Observatory OCO-2 (Osterman et al. 2016), and the Chinese Tansat; Yang et al.  
78 2018), but their focus is to observe and monitor atmospheric CO<sub>2</sub>. However, there is a suite  
79 of ocean observing satellite sensor datasets that could be used, through exploitation of

80 empirical relationships, to provide measures of marine carbonate chemistry parameters that  
81 include total alkalinity ( $A_T$ ), total dissolved inorganic carbon ( $C_T$ ), partial pressure of  $CO_2$  in  
82 seawater ( $pCO_2$ ) and pH (Gledhill *et al.*, 2009).

83

84 These four primary variables allow the ocean carbonate system to be investigated. In  
85 principle, knowledge of at least two of these four, in conjunction with temperature, salinity  
86 and pressure, allows the remaining variables to be calculated (Dickson and Riley, 1978). The  
87 relationships between these variables are principally driven by thermodynamics; temperature,  
88 pressure and salinity are therefore fundamentally associated with the carbonate system  
89 (Dickson, 2007). Furthermore, salinity is a significant driver of the ionic composition of  
90 seawater and hence has a strong relationship with  $A_T$  (Millero *et al.*, 1998). In addition to  
91 these physical controls on the carbonate system, the variables can be influenced by other  
92 chemical processes, including weathering and carbonate formation/dissolution (Friis *et al.*,  
93 2003), and biological processes such as primary production, respiration, calcification and  
94 remineralization (Smith *et al.*, 1975). With this knowledge it is possible to determine how the  
95 carbonate system variables vary in relation to factors such as temperature, salinity, nitrate or  
96 chlorophyll (the latter two as proxies for biological processes). These relationships take the  
97 form of empirical algorithms, which can be used to derive the respective carbonate system  
98 variable, and have been developed within a number of global and regional studies, e.g.  
99 Takahashi *et al.* (2013); Lee *et al.* (2006); Lee *et al.* (2000); Sasse *et al.* (2013); Cai *et al.*  
100 (2010); Lefèvre *et al.* (2010); Bonou *et al.* (2016); see Land *et al.* (2015) and references  
101 therein.

102

103 Although initially developed from *in situ* datasets, these empirical algorithms could  
104 potentially be forced with inputs from other sources, such as satellite observations or

105 climatologies to yield observation-based carbon system observations. Here we conduct a first  
106 assessment of four global algorithms for  $A_T$  and three for  $C_T$ , utilizing different combinations  
107 of satellite, interpolated *in situ* and climatology datasets as input. We then evaluate their  
108 output using independent *in situ* measurements of  $A_T$  and  $C_T$ . As a baseline comparison, we  
109 evaluate estimates of  $A_T$  and  $C_T$  from an Earth System model. In addition to the global  
110 algorithms, we also assess three regional  $A_T$  and two regional  $C_T$  algorithms. We aim to  
111 demonstrate algorithm suitability both globally and for regional case studies (the Caribbean,  
112 the Amazon plume and the Bay of Bengal), and to assess the performance of these different  
113 approaches, particularly the relevance of satellite datasets, in being able to reproduce the *in*  
114 *situ* patterns of these two carbonate system variables in surface waters.

115

## 116 **2. Materials and methods**

### 117 **2.1. Published algorithms**

118 The four global algorithms used here for  $A_T$  are from Lee *et al.* (2006) (hereafter referred to  
119 as L06), Takahashi and Sutherland (2013) (hereafter referred to as TS13) and Sasse et al  
120 (2013) (domain-based and global algorithms, hereafter referred to as S13 and S13g). L06  
121 separated the oceans into five domains and used an optimal polynomial fit to  $A_T$  data,  
122 resulting in a relationship with sea surface salinity (SSS) and sea surface temperature (SST)  
123 for each region. TS13 took this a step further using a larger combination of datasets to  
124 separate the oceans into 33 domains. Instead of using SST and SSS, TS13 assessed potential  
125 alkalinity relationship with SSS, where potential alkalinity is  $A_T$  plus nitrate concentration  
126 ( $\text{NO}_3$ ), which corrects  $A_T$  for the effect of changes in  $\text{NO}_3$  caused by net community  
127 utilization. Sasse et al (2013) used multiple linear regression to relate domain and global  $A_T$   
128 to SST, SSS,  $\text{SSS}^2$ , dissolved oxygen (DO), silicate (Si) and phosphate ( $\text{PO}_4$ ). The three  
129 regional  $A_T$  algorithms are all linear relationships with SSS using data from the Amazon

130 plume and Caribbean (Cai *et al.*, 2010; Lefèvre *et al.*, 2010). Two other regional algorithms  
131 (Cooley *et al.*, 2007; TERNON *et al.*, 2000) were considered, but were not used here as results  
132 differed only marginally from Lefèvre *et al.*, (2010) and they used much of the same training  
133 data.

134

135 The three global  $C_T$  algorithms that we used are from Lee *et al.* (2000) (hereafter referred to  
136 as L00) and Sasse *et al.* (2013) (domain-based and global algorithms, hereafter referred to as  
137 S13 and S13g). L00 found  $C_T$  normalized to salinity 35 on the Practical Salinity Scale and  
138 year 1990, ( $nC_T = C_T \times 35 / SSS + (\text{year} - 1990 \text{ between } 30^\circ\text{S and } 30^\circ\text{N})$ ), to be strongly  
139 correlated with SST and  $\text{NO}_3$ , and conducted optimal polynomial fitting for  $C_T$  to domain  
140 data, giving a total of 12 regionally parameterized equations. Sasse *et al.* (2013) used  
141 multiple linear regression to relate domain and global  $C_T$  to SST, SSS, DO,  $\text{NO}_3$ , Si and  $\text{PO}_4$ .  
142 The two regional  $C_T$  algorithms are both linear relationships with SSS using data from the  
143 Amazon plume (Lefèvre *et al.*, 2010; Bonou *et al.*, 2016). The same two regional studies as  
144 for  $A_T$  (Cooley *et al.*, 2007; TERNON *et al.*, 2000) were considered for  $C_T$ , but again results  
145 differed only marginally from those of Lefèvre *et al.*, (2010) and so they were not used.

146 In all cases, extrapolation of algorithms beyond the range for which they were calibrated is  
147 questionable, and this is especially true of nonlinear algorithms. To avoid this, we did not use  
148 any algorithm outside its specified range of applicability, or more than one SSS unit or SST  
149 degree outside its calibration range if a range of applicability is not specified. Table 1  
150 summarises the algorithm choices and dependences. Additional details on each empirical  
151 relationship for all algorithms are provided in Supporting Information Text S1.

152

## 153 **2.2. Round-robin comparison**



154 Four case study regions were used in a round-robin comparison of the algorithms: the global  
155 ocean, the Caribbean (14°N to 30°N, 90°W to 60°W for compatibility with Gledhill *et al.*  
156 (2008)), the Amazon plume (2°S to 22°N, 70°W to 32°W), and the Bay of Bengal (5°N to  
157 24°N, 78°E to 96°E, using the Bay of Bengal International Hydrographic Office Sea Area  
158 (International Hydrographic Organization, 1953)). These case studies were chosen as areas  
159 that are potentially challenging for this assessment and are discussed in more detail in Land *et*  
160 *al.*, (2015). The Amazon region was chosen to enclose the region of freshening contiguous  
161 with the mouth of the Amazon with any monthly satellite SSS < 35, with an eastern boundary  
162 at 32°W, beyond which rain freshening dominates the Amazon plume (Ibáñez *et al.*, 2016).  
163 The region defined also includes many points with SSS > 35. To investigate the effect of  
164 these points, we also defined a low-salinity Amazon region where data with *in situ* SSS > 35  
165 were excluded.

166

167 Each algorithm was tested using input data for each forcing factor (SSS, SST, NO<sub>3</sub>, DO, Si  
168 and/or PO<sub>4</sub>) from a range of data sources and all possible combinations of inputs were  
169 included in the round-robin comparison. The input data for the empirical algorithms were:

170 1) Monthly mean satellite observed data from the Soil Moisture and Ocean Salinity (SMOS)  
171 satellite [SSS 2010-2017 CATDS-IFR-CEC-v02] (Reul *et al.*, 2015), the Aquarius satellite  
172 [SSS 2011-2015, Version 5] (Le Vine *et al.*, 2014), and the Climate Change Initiative (CCI)  
173 [SST 1991-2010] (Merchant *et al.*, 2012);

174 2) *In situ* re-analysis data from the Coriolis Ocean Re-Analysis (CORA v4.3) database [SSS,  
175 SST 1990-2012] (Cabanès *et al.*, 2013);

176 3) Monthly climatology data from the World Ocean Atlas (WOA) dataset [SSS, SST, nitrate,  
177 DO, Si, PO<sub>4</sub>] (García *et al.*, 2010);

178 Note that WOA ‘nitrate’ is actually nitrate + nitrite ( $\text{NO}_3 + \text{NO}_2$ ). However,  $\text{NO}_2$  typically  
179 has a concentration at least an order of magnitude lower than  $\text{NO}_3$ , and so this discrepancy is  
180 neglected. The previously mentioned baseline comparison dataset were  $A_T$  and  $C_T$  output  
181 from the HadGEM2-ES global Earth system model, 1972-2020 (Jones *et al.*, 2011) (hereafter  
182 referred to as HG2).

183 All data were binned spatially to a  $1^\circ \times 1^\circ$  grid and temporally to monthly intervals (henceforth  
184 referred to as monthly data). The multi-year CORA, satellite and HG2 data were also each  
185 combined to form monthly climatologies (climatological data). Only  $1^\circ \times 1^\circ$  grid cells with at  
186 least two values were used to calculate climatological data. Details of all of these input  
187 datasets are provided in Table 2.

188

189 The binned  $A_T$  or  $C_T$  from each algorithm and input, herein referred to as ‘output’, and the  
190 binned output from HG2 were all evaluated (validated) against binned *in situ* data of the  
191 respective carbonate parameter. Data from the Global Data Analysis Project Version 2  
192 (GLODAPv2, 1972-2013) (Olsen *et al.*, 2016) were the primary *in situ* evaluation  
193 (validation) data used for both  $A_T$  and  $C_T$  evaluations, along with some additional regional *in*  
194 *situ* data (see Table 3). The GLODAPv2 dataset is a community compiled, merged and  
195 internally consistent global dataset. In all cases of *in situ* data, the mean measurement in the  
196 top 10 m water depth was used.

197

198 Following (Sasse *et al.* 2013), we attempted to separate the effects of terrigenous influences  
199 and sediment resuspension on the biogeochemistry of coastal waters from open ocean  
200 carbonate chemistry by calculating the minimum depth within each cell using the  
201 GEBCO\_08 one-minute grid ([www.gebco.net/](http://www.gebco.net/))

202 data\_and\_products/gridded\_bathymetry\_data/gebco\_one\_minute\_grid/, downloaded on  
203 December 14<sup>th</sup>, 2009) and repeating our analysis using only grid cells with minimum depth  
204 greater than 500 m. Again following (Sasse et al. 2013), we further separated terrigenous  
205 effects by calculating the minimum distance from the nearest coast within each cell using  
206 (<https://oceancolor.gsfc.nasa.gov/docs/distfromcoast/>, downloaded on October 5<sup>th</sup>, 2018) and  
207 repeated the analysis using only grid cells with both a minimum depth greater than 500 m and  
208 a minimum distance greater than 300 km. All three sets of results are included in  
209 Supplementary Information, but only data with both masks applied are presented here.

210

### 211 **2.3. Statistical measures**

#### 212 **2.3.1 Data uncertainties**

213 The GLODAPv2 analysis (Olsen *et al.*, 2016), the chosen reference validation dataset,  
214 includes an estimate of the maximum bias that exists between different instruments  
215 determined via a crossover analysis as 4 and 6  $\mu\text{mol kg}^{-1}$  for  $C_T$  and  $A_T$  respectively. Whereas  
216 a full uncertainty budget (i.e. a type A uncertainty estimate (BIPM, 2008) comprising a  
217 combination of bias and standard deviation of all measurements against a traceable standard)  
218 are not provided. Therefore in the absence of all components of the uncertainty information  
219 we assume nominal uncertainties of 0.5% for all *in situ*  $A_T$  and  $C_T$  (Bockmon *et al.*, 2015). It  
220 should be noted that due to relatively recent improvements in quality control we would  
221 expect older *in situ* measurements to have greater uncertainties and more recent  
222 measurements to have lesser, though this variation is difficult to quantify. For interest, the  
223 GLODAPv2 bias estimate stated above for a mean global  $A_T$  of 2450  $\mu\text{mol kg}^{-1}$  gives a  
224 potential bias around 0.2%. Uncertainties in the input (forcing) data (SST, SSS,  $\text{NO}_3$  and  
225 HG2  $A_T$  and  $C_T$ ) were not included in our analysis, since these are unknown for many of the  
226 input datasets. For interest only, the reported uncertainty in SMOS SSS is below  $\pm 0.3$  for a 30

227 day average over a  $100 \times 100$  km open ocean area (Reul *et al.*, 2012; Reul *et al.*, 2014) and  
228 can be below  $\pm 0.2$  for an 18 day average (Boutin *et al.*, 2018) or in certain evaporation-  
229 dominated regions, and for Aquarius SSS it is  $\pm 0.17$  for a monthly average over a  $150 \times 150$   
230 km open ocean area (Lagerloef *et al.*, 2015). Uncertainty in CCI SST is between  $\pm 0.1$  and  
231  $\pm 0.15$  K (Merchant *et al.*, 2014). However, we could find no uncertainty estimates for the  
232 CORA, WOA or HG2 datasets, and it would be inconsistent to apply uncertainties to some  
233 inputs and not others. We discuss the impact of this approach within Section 4.2.

234

235 The published algorithm uncertainties (as stated in the corresponding reference) for each  
236 algorithm were propagated through to the algorithm outputs. Following standard propagation  
237 methods (Taylor, 1997), *in situ* and algorithm uncertainties were combined assuming that  
238 they were uncorrelated (a sum of squares analysis), allowing weighted statistics to be  
239 calculated, with each data point weighted by the inverse of the sum of squared uncertainties.

240

### 241 **2.3.2 Evaluating output accuracy**

242 Output mean ( $\bar{x}_m$ ), standard deviation ( $\sigma_m$ ) and *in situ* carbonate data mean ( $\bar{x}_d$ ) and standard  
243 deviation ( $\sigma_d$ ) were calculated for each assessment, as well as root-mean-square-difference  
244 (RMSD), mean absolute difference (MAD), bias and point-to-point correlation (R) between  
245 output and the evaluation (GLODAPv2) *in situ* data. As a check, each of these statistics is  
246 presented both weighted and unweighted. Unweighted and weighted RMSD values were  
247 usually within about 10%, except in the case of global  $A_T$  using the TS13 algorithm, which  
248 includes regions with very different algorithm errors. Weighted statistics are used hereafter.

249

250 A potential problem with comparing outputs in this way is that different outputs overlap with  
251 different evaluation *in situ* data. Consider the plausible situation in which all outputs perform

252 poorly in coastal waters. All else being equal, an output that is not evaluated using coastal in  
253 situ data will produce better statistics than one that is. Therefore, to compare like with like, in  
254 each region we considered outputs in pairs, for a given pair calculating RMSD for each of the  
255 two outputs using only in situ evaluation matchups shared by both outputs. Each output is  
256 given a ‘score’ of  $\text{RMSD} / \text{RMSD}_{\text{min}}$ , 1 for the lower RMSD and  $\geq 1$  for the other. This is  
257 repeated for all possible pairs, then each output is given a ‘final score’ equal to the mean of  
258 all of its scores. To convert this to an estimate of RMSD, we chose a representative output as  
259 that with the lowest value of (weighted final score / number of matchups), i.e. the output with  
260 the best combination of performance and coverage. The weighted RMSD of this output  
261 ( $\text{RMSD}_{\text{rep}}$ ) was left unchanged and all other output weighted RMSDs in the region were set  
262 to  $\text{RMSD}_{\text{rep}} \times \text{final score} / (\text{final score})_{\text{rep}}$ , where  $(\text{final score})_{\text{rep}}$  is the final score of the  
263 representative output; this measure is henceforth referred to as RMSDe. Output results can be  
264 compared directly within a region, but comparison of output RMSDe between regions or  
265 carbonate parameters should be treated with caution. The above calculations could equally be  
266 done using MAD in place of RMSD, though we have not done this here.

267

### 268 ***2.3.2 Evaluating optimal combinations of output elements and importances***

269 To calculate the relative importance of different combinations of output elements (algorithms  
270 and/or data inputs) to the output comparison results, we calculated the best RMSDe when a  
271 given combination is excluded from all outputs, and divided it by the overall best RMSDe to  
272 give an RMSDe ratio. For example, the most effective single exclusion, with an RMSDe ratio  
273 of 1.022 (i.e. a 2.2% difference), is  $A_T$  using climatological CORA SSS in the Bay of Bengal.  
274 The best 13  $A_T$  outputs in the Bay of Bengal all use climatological CORA SSS. Conversely,  
275 the best output also uses monthly CCI SST but the second best uses WOA SST, so excluding  
276 monthly CCI SST has much less effect. Excluding WOA SST has no effect, since the best

277 output is still the one using monthly CCI SST. Having excluded climatological CORA SSS,  
278 the next 14 best  $A_T$  outputs all use the TS13 algorithm, so excluding climatological CORA  
279 SSS and TS13 has the largest effect among pairs of exclusions in this region. All possible  
280 combinations of exclusions were considered, ranked in order of number of elements  
281 excluded, then by RMSDe ratio.

282 The resulting comprehensive list is rather hard to read and interpret. To simplify, we created  
283 subsets of exclusions objectively considered as most significant. Criteria used were that the  
284 RMSDe ratio was greater than 1.01, the exclusions were either all SSS and/or SST inputs or  
285 all algorithms, and RMSDe ratio exceeded that of a subset of exclusions by  $>0.1\%$ . For  
286 example, excluding TS13 and SMOS SSS would not qualify, and excluding SMOS and  
287 Aquarius SSS would only qualify if its RMSDe ratio were greater than excluding only SMOS  
288 and only Aquarius by  $>0.1\%$ .

289

### 290 ***2.3.3 Comparing between carbonate parameters***

291 To compare between carbonate parameters in each region, we only considered *in situ*  
292 evaluation data points where both  $A_T$  and  $C_T$  values existed. For each data point and  
293 parameter, all outputs producing valid output were considered and the one with the best  
294 regional final score was chosen, noting the output-*in situ* difference for this output. The  
295 regional RMSD of each parameter was then calculated from the differences at all data points  
296 in the region.

297

## 298 **3. Results**

299 Results are summarized in Figure 1A and B, showing RMSDe for  $A_T$  and  $C_T$ , Table 4,  
300 showing statistics of the lowest-RMSDe output for each SSS source plus HG2 output in each  
301 region, and Table 5, showing selected importances. Figures 2 to 4 contain plots of output

302 versus evaluation (GLODAPv2) *in situ*  $A_T$ ,  $C_T$  and SSS data, with points with depth < 500m  
303 and > 300 km from the coast labeled. Alternative versions of Figures 1A and 1B for differing  
304 masks are shown in Figure S1. Supporting data (Land et al. 2019) consist of three data  
305 collections corresponding to all data, minimum depth 500 m, and minimum depth 500 m plus  
306 minimum distance to coast 300 km; matchup data, output statistics, details of output score  
307 calculations, spatial data results, importances of exclusions and the comparisons between  
308 carbonate parameters (also included in Supplementary Information) are included.  
309 Generally there is little to choose between the SSS sources (re-analysed *in situ* or satellite)  
310 apart from HG2, which performs less well in all regions, or between monthly and  
311 climatological SSS sources. The main differences in performance are between algorithms and  
312 between regions, but there is no clearly superior algorithm.

313

### 314 **3.1. Total Alkalinity ( $A_T$ )**

315 See Table 4 for detailed results. Globally, the best RMSDe values of about  $17 \mu\text{mol kg}^{-1}$  are  
316 substantially lower than the SD of the global coverage *in situ* data used for the evaluation ( $81$   
317  $\mu\text{mol kg}^{-1}$ ), and in the Amazon and Bay of Bengal they are slightly lower (RMSDe of 55  
318 compared to a SD of 68, and RMSDe of 11 compared to a SD of  $16 \mu\text{mol kg}^{-1}$ , respectively),  
319 but in the Greater Caribbean and low-salinity Amazon the RMSDe are higher than the SD,  
320 meaning that none of the tested combinations of algorithms and inputs is accurate enough to  
321 distinguish natural variations in  $A_T$  in these latter two regions.

322

#### 323 **3.1.1. $A_T$ algorithm and input importances**

324 See Table 5 for details. Globally, S13 performs slightly less well (higher RMSDe) than other  
325 algorithms, as do climatological satellite inputs. In the Greater Caribbean, monthly SMOS  
326 and Aquarius and climatological Aquarius SSS perform significantly less well. In the

327 Amazon, the Lefevre et al (2010) algorithm and climatological Aquarius and WOA SSS  
328 perform less well. In the low-salinity Amazon, monthly SMOS and Aquarius and monthly  
329 CCI SST perform best. In the Bay of Bengal, climatological CORA SSS performs best and  
330 climatological Aquarius performs significantly less well.

331

### 332 3.1.2. $A_T$ summary

333 For all case study regions and with respect to these empirical outputs, satellite SSS can  
334 reproduce *in situ* measured  $A_T$  from the GLODAPv2 evaluation dataset with performance  
335 (RMSDe) comparable to, or better than, the re-analysed *in situ* data derived inputs for SSS,  
336 and the satellite based  $A_T$  is always better than HG2  $A_T$  estimates. Globally HG2  
337 performance is about 85% worse than the best SSS driven outputs, but this reduces to 15-  
338 20% in the Amazon plume. Monthly Aquarius and SMOS observations provide a credible  
339 solution to monitoring synoptic scale global and regional  $A_T$ , though in some challenging  
340 regions (Greater Caribbean and low-salinity Amazon plume) none of the tested methods are  
341 sufficiently accurate to resolve natural variability.

342

343 RMSDe in the Amazon plume is higher than the global RMSDe, reflecting the larger regional  
344 standard deviation in the *in situ* data due to the large gradients around the river flow, and  
345 RMSDe in the Amazon with SSS < 35 is higher than in the wider Amazon, but the relative  
346 performance of SSS inputs is similar.

347 Excluding the Amazon plume and HG2, the best outputs have bias less than  $5 \mu\text{mol kg}^{-1}$ , or  
348 0.2% of the global mean  $A_T$  (of  $2450 \mu\text{mol kg}^{-1}$ ) which is similar to the estimated evaluation  
349 dataset *in situ* nominal uncertainty of 0.5% (Bockmon *et al.*, 2015) and the inter-annual  
350 variability of  $A_T$  observed at oceanic sites such as at the Hawaiian Ocean Time-series station  
351 (HOT;  $\pm 6 \mu\text{mol kg}^{-1}$ ) (Brix *et al.*, 2004), but lower than the seasonal variability observed at



352 oceanic sites (20 to 30  $\mu\text{mol kg}^{-1}$  at both the Bermuda Atlantic Time-series Study (BATS)  
353 (Bates *et al.*, 2012) and the European time series station (ESTOC) (Santana-Casiano *et al.*,  
354 2007). This seasonal variability at BATS and ESTOC is also greater than the best global  
355 RMSDe of 17  $\mu\text{mol kg}^{-1}$ . In the Amazon plume, of the monthly SSS sources only SMOS has  
356 low bias (2  $\mu\text{mol kg}^{-1}$ ), and in the low-salinity Amazon plume, all SSS sources have bias  
357 greater than 19  $\mu\text{mol kg}^{-1}$ . These results highlight that these methods (of using satellite  
358 observations or re-analysed *in situ* dataset as input to empirical algorithms) can obtain  
359 measures of  $A_T$  that are not significantly biased relative to the evaluation *in situ*  
360 measurements, except in regions of strong spatiotemporal variability. It also shows that these  
361 methods are capable of distinguishing the seasonal variability at long-term time series sites,  
362 though not the interannual variability at HOT.

363

### 364 **3.2. Total Dissolved Inorganic Carbon ( $C_T$ )**

365 See Table 4 for detailed results. Globally, the best RMSDe values of 29-30  $\mu\text{mol kg}^{-1}$  are  
366 considerably higher than the equivalent global  $A_T$  RMSDe values, but still substantially  
367 lower than the SD of the global *in situ* evaluation dataset (69  $\mu\text{mol kg}^{-1}$ ), and in the Amazon  
368 and Greater Caribbean they are similar (RMSDe 45 compared to SD 53 and RMSDe 19  
369 compared to SD 18  $\mu\text{mol kg}^{-1}$ , respectively), but in the low-salinity Amazon and Bay of  
370 Bengal they are higher, meaning that no combination of algorithms and inputs is accurate  
371 enough to distinguish natural variations in  $C_T$  in these latter two regions.

#### 372 **3.2.1. $C_T$ algorithm and input importances**

373 See Table 5 for details. Globally, L00 and S13g perform better (lower RMSDe) than other  
374 algorithms, as do CORA, WOA and monthly SMOS SSS inputs. In the Greater Caribbean,  
375 the S13g algorithm performs very poorly and climatological Aquarius SSS performs less well  
376 than other SSS inputs. In the Amazon, the S13g algorithm and Aquarius SSS perform less

377 well. In the low-salinity Amazon, the S13g algorithm performs less well, while SMOS,  
378 Aquarius and monthly CCI SST perform best. In the Bay of Bengal, the S13 and S13g  
379 algorithms perform considerably better than other algorithms and CORA and WOA SSS  
380 perform better than other SSS sources.

381

### 382 3.2.2. $C_T$ summary

383 Similar to  $A_T$ , satellite inputs for SSS can reproduce the  $C_T$  data (from the GLODAPv2  
384 evaluation dataset) with similar ability, and sometimes better than using re-analysed or  
385 climatology *in situ* derived SSS inputs, except for Aquarius in the Amazon plume (Figure  
386 1B), and always better than HG2  $C_T$  estimates. Global HG2 performance is only about 14%  
387 worse than the best SSS driven outputs, but this increases to over 80% in the Bay of Bengal  
388 and Greater Caribbean. As with  $A_T$ , monthly SMOS and Aquarius observations provide a  
389 credible solution to monitoring synoptic scale global and in some cases regional  $C_T$ . Best  
390 RMSDe values are higher for  $C_T$  than  $A_T$  globally and in the Greater Caribbean and Bay of  
391 Bengal, but lower in both Amazon plume regions. Again, in some challenging regions (low-  
392 salinity Amazon plume and Bay of Bengal), none of the tested methods are sufficiently  
393 accurate to reproduce natural variations.

394

395 Bias in the  $C_T$  outputs is generally greater and more variable than that in the  $A_T$  outputs,  
396 except in the Amazon plume where non-HG2 monthly and climatological bias is uniformly  
397 less than  $3 \mu\text{mol kg}^{-1}$ . The smallest bias among the best global monthly outputs is monthly  
398 CORA with  $-9 \mu\text{mol kg}^{-1}$ , in the Greater Caribbean monthly SMOS and Aquarius have bias  
399 of 3 and  $4 \mu\text{mol kg}^{-1}$  respectively, monthly outputs in the low-salinity Amazon are all  
400 strongly biased, the smallest being CORA with  $45 \mu\text{mol kg}^{-1}$ , and in the Bay of Bengal  
401 monthly CORA has bias of  $16 \mu\text{mol kg}^{-1}$  while climatological datasets (WOA, CORA,

402 SMOS) have lower bias (-11, -12, -14  $\mu\text{mol kg}^{-1}$  respectively). For comparison, the *in situ*  
403 nominal uncertainty of 0.5% (Bockmon *et al.*, 2015) at the global average  $C_T$  of 1900  $\mu\text{mol}$   
404  $\text{kg}^{-1}$  would be 9.5  $\mu\text{mol kg}^{-1}$ , the inter-annual variability of  $nC_T$  is  $\pm 4 \mu\text{mol kg}^{-1}$  at HOT and  
405  $\pm 8 \mu\text{mol kg}^{-1}$  at ESTOC (Brix *et al.*, 2004, Santana-Casiano *et al.*, 2007), while the seasonal  
406 amplitude of  $nC_T$  at HOT is 15  $\mu\text{mol kg}^{-1}$  (Brix *et al.*, 2004) and those of  $C_T$  at ESTOC and  
407 BATS are 20-30 and 40-50  $\mu\text{mol kg}^{-1}$ , respectively (Santana-Casiano *et al.*, 2007, Bates *et*  
408 *al.*, 2012). The biases in these outputs are also comparable to the systematic biases found by  
409 Lee *et al.* (2000) when comparing algorithm derived  $nC_T$  to  $nC_T$  calculated from  $A_T$  and  
410  $p\text{CO}_2$  data (-3 to +15  $\mu\text{mol kg}^{-1}$ ). Thus, these results highlight that some of the outputs  
411 evaluated can obtain measures of  $C_T$  that are not significantly biased relative to the *in situ*  
412 evaluation measurements, though overall uncertainties may be high relative to the variability  
413 at these long-term monitoring sites.

414

### 415 3.3. $A_T$ and $C_T$ Algorithm biases

416 In the Amazon Plume, the best output was strongly correlated with the evaluation *in situ*  $A_T$   
417 or  $C_T$ , but with a slope significantly different from 1 (Figures 2B and 3B). Replacing monthly  
418 satellite SSS with monthly or climatological CORA SSS (re-analysed and interpolated *in*  
419 *situ*) produces similar biases (Figure 4), suggesting that the cause of the bias is not specific to  
420 satellite SSS or monthly data.

421

422 A possible explanation of this bias would be that the algorithm is not capturing the two  
423 endmember mixing from the river with zero salinity and some finite, but significant  $A_T$  and  
424  $C_T$ . However, the regional algorithms for the Amazon plume implicitly include the river  
425 endmember, as they are based on measurements that include low and high salinity values,  
426 and each published algorithm finds a strongly linear relationship between salinity and  $A_T$  or

427  $C_T$ . Since the bias using these algorithms is similar to that using the global algorithms, we can  
428 conclude that the endmember issue is not the main reason for the bias.

429

430 Another possible explanation of the bias would be sampling of water with low SSS,  $A_T$  and  
431  $C_T$  in regions with high spatial and temporal SSS variability, as found in the Amazon plume  
432 and particularly within the low salinity Amazon plume region. Satellite and CORA data  
433 represent an average over at best one grid cell (about  $10^4$  square kilometers at the equator)  
434 and one month (or the same month in a range of years in the case of climatological data),  
435 while an *in situ* measurement samples a very small volume of water and is almost  
436 instantaneous. The effect of this averaging is to remove variability that occurs on smaller  
437 spatial and temporal scales. For example, low *in situ* salinity in the Amazon plume may be  
438 caused by small eddies or filaments of river water not resolvable at the grid cell scale, or by  
439 interannual variations in the plume extent. In this situation, extreme evaluation *in situ* values  
440 will consistently be matched with outputs driven by satellite and CORA data that are closer to  
441 the large-scale and long-term mean. If the salinity distribution is strongly one-tailed, as in the  
442 Amazon plume, and the cause of anomalies is consistently unresolved by the averaged data,  
443 the *in situ* evaluation data will consistently give lower salinity than the averaged data, as  
444 observed here (Figure 5). This issue is likely to be one cause of the large biases evident in all  
445 output results (re-analysed *in situ* and satellite input derived) for the low salinity Amazon  
446 region.

447

448 A third possible explanation for the bias arises from fundamental differences between the *in*  
449 *situ* measurements used to calibrate the original algorithms and the satellite salinity  
450 observations used herein as input to the algorithms. Satellite SSS observations represent the  
451 conditions in the top 10 mm of the water (Boutin *et al.*, 2013), whereas *in situ* SSS

452 observations are typically sampled from  $\geq 1$  m below the surface. This can result in  
453 geophysical sources of variation between satellite and *in situ* salinity, which are linked to  
454 vertical salinity stratification, and these features are prevalent in regions of rain, oceanic  
455 fronts and river outflow (Boutin *et al.*, 2013; Boutin *et al.*, 2016; Drucker *et al.*, 2014). For  
456 example, salinity gradients created by freshwater plumes can complicate the comparison of  
457 satellite and *in situ* salinity measurements; a difference of 2–5 pss  $\text{m}^{-1}$  has been observed  
458 across the halocline in the Amazon plume (Lentz *et al.*, 1995). Plumes can also cause  
459 horizontal salinity gradients with spatial scales smaller than the footprint of the satellite  
460 radiometers. Typical horizontal SSS gradients for the plumes from the Amazon (Lentz *et al.*,  
461 1995) or Congo (Chao *et al.*, 2015) exceed 0.2 pss  $\text{km}^{-1}$  and extend more than 250 km from  
462 the river mouth. Therefore, in the vicinity of a river plume, a spatially sparse array of *in situ*  
463 sensors can exhibit very different SSS variability from that observed by a satellite sensor,  
464 even if the measurements are all coincident. Similarly, high-frequency SSS variations (e.g.  
465 tidal effects) can be undersampled by satellite-derived SSS products due to the relatively long  
466 revisit time of the satellite (2–3 days for SMOS and 7 days for Aquarius). Accounting for the  
467 depth-related differences should increase the accuracy of the outputs, and a rigorous  
468 treatment might adapt the theory currently used to reconcile *in situ* and satellite SST  
469 (Merchant *et al.*, 2014). We therefore recommend that the satellite SSS community consider  
470 investigating this theory for SSS.

471

472 In the absence of a rigorously tested explanation for these biases, and to demonstrate the  
473 potential gain from reducing them, we simply note that linear regression of the best output  
474 against the evaluation *in situ*  $A_T$  and  $C_T$  reduces the RMSD (actual, not estimated) in the low  
475 salinity Amazon plume region from 215 to 48  $\mu\text{mol kg}^{-1}$  (a 77% reduction) for  $A_T$  and from  
476 67 to 50  $\mu\text{mol kg}^{-1}$  (26%) for  $C_T$ .

477

#### 478 **3.4. Comparison of $A_T$ with $C_T$**

479 Results are shown in Dataset S23, showing that in direct comparisons at each matchup  
480 position, the  $A_T$  outputs have a 42% lower RMSDe than  $C_T$  globally, 41% lower in the Bay  
481 of Bengal and 21% lower in the Caribbean, indicating that  $A_T$  outputs can generally be  
482 retrieved more successfully than  $C_T$  outputs. However,  $A_T$  has a 13% higher RMSDe than  $C_T$   
483 in the Amazon and 9% higher in the low salinity Amazon using the same algorithms as in the  
484 global case, so this relationship is not universal.

485

#### 486 **3.5. Multi-year synoptic observations**

487 The methods evaluated here enable the first multi-year synoptic scale observations of  $A_T$  and  
488  $C_T$  spatial mixing and distributions. To demonstrate their application we characterise the  
489 synoptic scale, extent and influence of river-flow-dominated alkalinity mixing in the Amazon  
490 plume and western North Atlantic. The Amazon Plume exhibits a two-end-member  
491 alkalinity-salinity mixing regime, resulting in a strong linear relationship between alkalinity  
492 and salinity (Cai *et al.*, 2010), and mixing between river water and seawater is the dominant  
493 controlling factor of the alkalinity-salinity relationship in the western North Atlantic (Jiang *et*  
494 *al.*, 2014). The accuracy assessment means that we can illustrate SMOS or Aquarius  
495 observational-based  $C_T$  and  $A_T$  monitoring of the Amazon plume along with a calculated  
496 estimate of the combined uncertainty in  $C_T$  and  $A_T$  (provided by the RMSDe and bias).

497

498 To simplify the interpretation we present results using the same algorithm for monthly SMOS  
499 and Aquarius, so that any differences are due solely to the SSS source. For  $A_T$ , the best  
500 output with both SMOS and Aquarius is TS13 with WOA nitrate, with RMSDe of 57.7  $\mu\text{mol}$   
501  $\text{kg}^{-1}$  for SMOS and 58.4  $\mu\text{mol kg}^{-1}$  for Aquarius. For  $C_T$  the best Aquarius outputs use

502 different algorithms to the best SMOS outputs, and perform less well. Therefore for  
503 simplicity we present results of using SMOS and Aquarius with a single algorithm and input  
504 pairing (L00 and climatological CORA SST), with RMSDe of  $45.0 \mu\text{mol kg}^{-1}$  for SMOS and  
505  $52.2 \mu\text{mol kg}^{-1}$  for Aquarius. We calculated  $A_T$  and  $C_T$  time series for the Amazon plume  
506 using the above algorithm and input pairings, producing monthly Aquarius and SMOS  
507 derived  $A_T$  and  $C_T$  collectively covering the time period 2010 to 2016.

508

509 Figure 6 shows the regional ( $0-15^\circ\text{N}$ ,  $45-62^\circ\text{W}$ ) mean SMOS and Aquarius SSS,  
510 climatological CORA SST, output  $A_T$  and output  $C_T$ , in relation to climatological Amazon  
511 discharge data from the Obidos gauge located 750 km from the ocean (Perry *et al.*, 1996).  
512 The discharge data are only provided as an indication of variations in Amazon discharge and  
513 will not represent the total flow (Salisbury *et al.*, 2011). In a given month with both SMOS  
514 and Aquarius data, we calculate mean SSS using only cells in which both have valid data, in  
515 order to compare like with like. If this is not done, and one dataset extends into a low salinity  
516 region not covered by the other, large spurious differences can occur, e.g. in May 2014  
517 inconsistent masking causes the regional mean Aquarius SSS to be 1.24 units lower than  
518 SMOS SSS (results not shown), a difference that reduced to 0.07 units with consistent  
519 masking. Maximum SSS consistently occurs during December and January and minimum  
520 SSS occurs during May-July, 1-3 months after the maximum discharge in April, both of  
521 which are consistent with previous findings (Salisbury *et al.*, 2011). As expected,  $A_T$  and  $C_T$   
522 maxima occur in phase with the variations in SSS, and typically lag the peaks in SST by one  
523 to two months, with regional  $A_T$  each year varying between 2230 and  $2370 \mu\text{mol kg}^{-1}$  and  $C_T$   
524 varying between 1890 and  $2000 \mu\text{mol kg}^{-1}$ .

525

526 Figure 7 reveals the seasonal patterns in  $A_T$  over the same period as shown in Figure 6B in  
527 relation to the dynamics of the Amazon discharge and their interaction offshore with the  
528 along-shore North Brazilian Current, North Equatorial Counter Current and Guyana Current.  
529 The August 2011 SSS conditions are shown in Figure 7A. Clear annual cycles and river  
530 plume features are apparent in the observed  $A_T$ , with the Amazon plume influencing  $A_T$  more  
531 than 1000 km offshore of the mouth of the Amazon (Figure 7B-D). During June-July each  
532 year, very low  $A_T$  values reaching below  $2100 \mu\text{mol kg}^{-1}$  are apparent at the mouth of the  
533 Amazon (Figure 7D), the timing of which is consistent with the observed annual minima in  
534 SSS (Salisbury *et al.*, 2011) (see also Figure 6). Further west the river plume spreads out as it  
535 interacts with the along-shore currents, resulting in  $A_T$  in the region of  $\sim 2150 \mu\text{mol kg}^{-1}$  up to  
536  $\sim 1700$  km offshore (regions of yellow up to  $\sim 17^\circ\text{N}$  in Fig. 3C). The Amazon plume has been  
537 observed to bifurcate during the northern hemisphere summer months (Del Vecchio *et al.*,  
538 2004), with one part of the river plume heading north-west and a second jet retroflected to the  
539 east (Salisbury *et al.*, 2011). This bifurcation is apparent each year around August (Figure  
540 7A-D), with an isolated feature of  $A_T$  around  $2000\text{-}2100 \mu\text{mol kg}^{-1}$  appearing 500-1000 km  
541 offshore and to the east of the river mouth, although this feature was less pronounced during  
542 2014 (regions of yellow between  $5\text{-}10^\circ\text{N}$  in Figure 7D).

543

544 Figure 8 shows Aquarius and SMOS monthly  $A_T$  for April 2012 overlaid with 100 *in situ*  $A_T$   
545 observations from the GLODAPv2 dataset (Olsen *et al.*, 2016) collected at 3 m nominal  
546 depth during 13 consecutive days in April and May 2012, and Figure 9 shows the equivalent  
547 plot for  $C_T$ . Despite the different temporal resolutions, the change in magnitude of the  
548 observations (the gradient) between the open ocean data and those close to, and within the  
549 river plume, are generally comparable to the synoptic scale observations. The high monthly  
550 temporal variations along the  $\sim 52^\circ\text{W}$  latitudinal transect are illustrated in Figure 7D. The



551 differences between *in situ* and synoptic scale observations are discussed in section 3.3. This  
552 comparison highlights the power of the synoptic scale observations, allowing the *in situ*  
553 observations to be placed within their wider spatial and temporal context. It also highlights  
554 how the synoptic observations characterise the distributions and mixing at the very surface of  
555 the water column and how these can be different from that observed *in situ* (at a nominal  
556 depth of 3 m), particularly in regions of strong river plume influence. Figures 8 and 9 could  
557 suggest that lower values of  $A_T$  and  $C_T$  are found below the surface in the coastal region,  
558 whereas offshore the salinity,  $A_T$  and  $C_T$  are vertically well mixed. A combination of *in situ*  
559 and synoptic scale observations could be used to understand the near-surface vertical profile  
560 of  $A_T$ .

561

## 562 **4.0 Discussion**

### 563 **4.1 Bay of Bengal**

564 Because there are permanent and strong radio-frequency interference sources around the  
565 coasts of Asia, SSS measurements from SMOS and Aquarius are likely to be of a lower  
566 quality in the Bay of Bengal. However, the paucity of *in situ* measurements in the Bay of  
567 Bengal in the satellite salinity era makes comparison difficult. The Bay of Bengal *in situ*  $A_T$   
568 data measured in 2014 were not included in the main analysis due to their proximity to the  
569 coast (and so were removed due to the masking), and their inclusion causes the RMSDe of  
570 HG2 to increase to over  $600 \mu\text{mol kg}^{-1}$  (Figure S1). This demonstrates the importance of  
571 comparing like with like when evaluating the outputs and also highlights the influence of  
572 focusing on evaluation data without terrigenous influence. The low number of *in situ* data  
573 points used in the Bay of Bengal accuracy assessment highlights that the evaluation of output  
574 datasets (from both satellites and re-analysed *in situ*) will be biased against small-scale  
575 variability that may be captured by the *in situ* observation data used for the evaluation,

576 particularly when *in situ* validation sites are relatively near-shore and the effect of riverine  
577 water flow is more pronounced. This was the case for the 2014 *in situ* dataset that was  
578 omitted from the main accuracy assessment due to falling within the masked area: the site  
579 was part of the Sundarbans Biological Observatory Time Series, representing the coastal part  
580 of the Sundarbans mangrove ecoregion, which can act as a source and a sink of CO<sub>2</sub> during  
581 pre-monsoon (April-May) (Akhand *et al.*, 2017), and it is also an area that receives high  
582 freshwater discharge (~42000 m<sup>3</sup> s<sup>-1</sup>) along with local heavy seasonal precipitation, in  
583 addition to increasing anthropogenic pressure (Choudhury *et al.*, 2015). The other case study  
584 regions have more data available for comparison and therefore this variability may be  
585 averaged out in the *in situ* data binning process. It is essential that more *in situ* carbonate  
586 system data are collected to elucidate these issues for this complex region (the Bay of  
587 Bengal), which has a strong riverine influence, and to characterize the variability on a wider  
588 scale than has currently been observed (Sarma *et al.*, 2012; Samanta *et al.*, 2015).

589

590 A large area of the Bay of Bengal is characterized by pCO<sub>2</sub> levels far below the atmospheric  
591 value (i.e. a large gradient between atmospheric and oceanic pCO<sub>2</sub>), which is more prominent  
592 during the north-east monsoon when the air-sea pCO<sub>2</sub> gradient exceeds 100 µatm (Akhand *et*  
593 *al.*, 2013; Ganguly *et al.*, 2011). The enhanced gradient is possibly due to new biological  
594 production sustained by excessive nutrient inputs from the Ganga-Brahmaputra-Meghna river  
595 basins, thus influencing the carbonate system via net organic production. Additionally, the  
596 presence of non-carbonate alkalinity in these regions (e.g. riverine contributions of organic  
597 species including humic acid) can result in A<sub>T</sub> that is not correlated with salinity (Akhand *et*  
598 *al.*, 2013). Only 14 of the outputs overlapped in space and time with the 2014 *in situ* data that  
599 captured this very near-shore variability, resulting in the apparent poor performance of these  
600 14 outputs before coastal masking. If the other outputs had also captured this near-shore

601 variability they may also have had reduced performance. Low satellite SSS coverage due to  
602 the issues of radio-frequency interference described above will have also contributed to lower  
603 performance of the satellite data driven outputs in this region. Improvements in satellite data  
604 coverage in coastal regions together with increased *in situ* data are likely to begin resolving  
605 these issues.

606

#### 607 **4.2 The need for continued efforts in quantifying uncertainties**

608 The problem of uncertainties, and their propagation through the analysis, is an ongoing one.  
609 Here, the estimated uncertainties in the *in situ* measurements used for the evaluation and  
610 algorithm uncertainties were included in the analysis where they were quantifiable (i.e.  
611 nominal uncertainties for the  $C_T$  and  $A_T$  *in situ* evaluation measurements and the propagation  
612 of the empirical algorithm uncertainties). Published remote sensing uncertainties are  
613 available, however no such information exists for the other input datasets; and even within  
614 the carbonate system there are still many challenges to fully defining *in situ* and laboratory  
615 measurement uncertainties (Andrew Dickson, pers. comms.; Bockmon and Dickson, 2015).  
616 Therefore, quantification of associated uncertainties for all of the input data sources requires  
617 continued work. Furthermore, unavoidably in this analysis, data used to evaluate the  
618 algorithm outputs were unlikely to be wholly independent from the data used to create the  
619 algorithms. In order to have a fully independent evaluation dataset, original datasets would be  
620 required to develop the algorithms whilst keeping enough data separate from the algorithm  
621 development process to enable an independent evaluation. This was not possible in this initial  
622 assessment due to the general dearth of measurements in some regions, and due to ambiguity  
623 over which measurements were used to develop the historical algorithms.

624

625 However in relation to our calculated combined uncertainties of our outputs, the estimated  
626 combined uncertainties from Fine *et al.* (2017) of smaller than  $\pm 20 \mu\text{mol kg}^{-1}$  for retrieving  
627 global  $A_T$  using satellite salinity and SST are consistent with our global results of RMSDe of  
628  $17 \mu\text{mol kg}^{-1}$ , bias  $< 5 \mu\text{mol kg}^{-1}$ . This gives further confidence in the approach taken here.  
629 We note however that Fine *et al.* (2017) misinterpreted the uncertainty information provided  
630 by Olsen *et al.*, (2016), as Olsen *et al.* only state the bias, which as previously discussed is  
631 only one component of a Type A uncertainty.

632

633 To test the sensitivity of the output uncertainties to the SST and SSS satellite remote sensing  
634 input data uncertainties, the latter were propagated through the analysis for all global  
635 empirical  $A_T$  algorithms (TS13, Lee06, Lee00, S13, S13g) for two example months (January  
636 and July). This results in  $A_T$  output uncertainties (due solely to satellite SSS and SST input  
637 data) of 0.2 to 0.8% (Table 6), which is close to the nominal *in situ* uncertainties of 0.5%, or  
638  $\pm 10 \mu\text{mol kg}^{-1}$ . The combined uncertainty in most of the studied regions is considerably  
639 greater than this, implying that (in the global case at least) the other components of the  
640 uncertainty budget dominate over the remote sensing input data uncertainty.

641

### 642 **4.3 The need for algorithm retraining and the collection of *in situ* observations**

643 Only seven global and five regional algorithms were presented here, in addition to output of  
644  $A_T$  and  $C_T$  from HG2, primarily because these were the only algorithms from the published  
645 literature that did not require additional re-parameterization for all the case study regions.  
646 Future efforts are needed to perform this re-fitting, not only for additional  $A_T$  and  $C_T$   
647 algorithms, but also for the remaining carbonate system parameters ( $p\text{CO}_2$  and pH). This is a  
648 demanding task; with just the 14 algorithms and model outputs used here, 1070 outputs were  
649 compared in the round-robin comparisons. Further, where few *in situ* measurements of a

650 carbonate variable exist (e.g. pH), information could be obtained for future assessments by  
651 calculating this variable from two of the other carbonate variables (e.g.  $C_T$  and  $A_T$ ) along with  
652 temperature and salinity. Calculating the variable in this way does introduce additional  
653 uncertainties, thus to be truly beneficial, such outputs should include the propagation of all  
654 uncertainties. A future assessment of the exploitation of satellite SSS will require further  
655 analysis of temporally resolved (rather than climatological) satellite observations, using new  
656 *in situ* data. We found only three cruises within GLODAPv2 that overlap with satellite  
657 salinity observations in our regions: none in the Bay of Bengal, one in the Amazon plume at  
658 the beginning of May 2010 (the first month of reliable SMOS data after its launch in  
659 November 2009) and two in the Amazon plume in April and May 2012 (shown in Figures 8  
660 and 9), one of which overlapped with the Greater Caribbean (only 6% and 3% of the  
661 GLODAPv2 data correspond to SMOS and Aquarius eras respectively). Hence coverage  
662 where we have both *in situ* and satellite observations is very limited spatially, seasonally and  
663 interannually, highlighting the need for further *in situ* data. It should also be noted that the  
664 lowest uncertainties achieved using these satellite observation-based and empirical  
665 approaches are still greater than the nominal *in situ* and laboratory measurement uncertainties  
666 (of  $\pm 10 \mu\text{mol kg}^{-1}$ ) so the methods presented here are unlikely to ever be a substitute for *in*  
667 *situ* measurements. Their strength is in providing synoptic data to fill the inevitable gaps in  
668 the *in situ* data coverage. To enable all new *in situ* data to be fully exploited by the Earth  
669 observation community they need to have been collected following international protocols (as  
670 defined by Dickson et al., 2007), analysed using traceable standards (as advocated by  
671 Bockmon and Dickson, 2015) enabling the provision of a complete uncertainty budget  
672 (quantified as a Type A uncertainty, BIPM, 2008). If possible, the historical data contained  
673 within the GLODAPv2 dataset would benefit from the inclusion of some indication of their  
674 uncertainty budget e.g. a simple ‘high’, ‘low’ or ‘unknown’ determined using existing

675 metadata and/or expert interpretation and opinion via a Type B uncertainty approach as  
676 defined by BIPM, (2008). Similarly, the CORA re-analysis and WOA climatology data  
677 would benefit from similar additions as these datasets lack any uncertainty information.

678

#### 679 **4.4 Earth system model performance**

680 It should be noted that we would not expect a free running global Earth system model such as  
681 HG2 to perform well regionally, though the poor global  $A_T$  performance and the relatively  
682 good performance in the Amazon plume were surprising. We include HG2 in the comparison  
683 mainly to illustrate how this methodology could be used to compare model data with quite  
684 different input sources such as satellite data. Our results provide a potentially useful dataset  
685 (including uncertainty information) to evaluate and challenge Earth system model outputs.

686

### 687 **5. Conclusions**

688 We demonstrate that satellite SSS and SST data are, in conjunction with empirical  
689 algorithms, able to successfully reproduce both  $A_T$  and  $C_T$  in four regions (globally, the  
690 Caribbean, the Amazon and the low salinity Amazon) as well as or better than *in situ*-derived  
691 (re-analysed) SSS and SST using the same empirical algorithms, or a global Earth system  
692 model dataset, with the advantage that satellite datasets are acquired daily, on average, with  
693 synoptic coverage.

694 The ability to derive key surface carbonate system parameters from satellite observed SSS  
695 and SST offers the potential for quantifying natural variability, as well as monitoring the  
696 present state of these important parameters through space and time. Satellite sensors provide  
697 a significant advantage over traditional *in situ* derived climatologies because of the ability to  
698 provide synoptic and frequent observations of global oceans. Critically, many of the satellites  
699 that provide these data are already in operation, hence historic satellite sensor datasets could

700 be used with these algorithms to elucidate changes over longer periods of time. These  
701 satellite methods should not replace ongoing *in situ* measurements, but should complement  
702 and enhance them by providing observations in periods where there are gaps in both time and  
703 space. Ongoing *in situ* data are essential to improve our ability to exploit satellite data, for  
704 example through enhanced parameterization of the algorithms. Satellites are also only able to  
705 measure surface waters, and are unable to measure under ice. These gaps must be filled with  
706 *in situ* data. Similarly, the evolving nature of the carbonate system due to anthropogenic  
707 forcing means that it is likely that these empirical algorithms will need to be periodically re-  
708 trained to maintain their performance. Hence the algorithms and methods utilized are useful  
709 for studying seasonal and inter-annual variations and episodic events, but may not be suitable  
710 for resolving longer-term trends.

711

712 The assessment presented here, which represents a significant effort and extensive analysis,  
713 provides the baseline performance against which any future algorithm re-training or re-  
714 calibration attempts can be compared.

715

## 716 **Acknowledgments**

717 This work was funded by the European Space Agency (ESA) Support to Science Element  
718 (STSE) Pathfinders Ocean Acidification project (contract No. 4000110778/14/I-BG,  
719 <http://www.pathfinders-oceanacidification.org/>) with additional support from the ESA  
720 Satellite Oceanographic Datasets for Acidification, OceanSODA, (contract No.  
721 4000112091/14/I-LG, <https://www.esa-oceansoda.org/>). The authors thank Professor Andrew  
722 Dickson, Scripps Institution of Oceanography, for discussions about carbonate chemistry  
723 uncertainties and error propagation.

724

725 **Tables**

726 Table 1: Summary of algorithms, their dependencies and the region for which they were  
 727 originally developed.  $A_T$  = Total Alkalinity,  $C_T$  = Dissolved Inorganic Carbon; SSS = Sea  
 728 Surface Salinity, SST = Sea Surface Temperature, DO = Dissolved Oxygen, N = nitrate, Si =  
 729 silicate, P = phosphate.

| Product | Name | Dependencies              | Reference                       | Region   |
|---------|------|---------------------------|---------------------------------|----------|
| $A_T$   | TS13 | SSS, N                    | (Takahashi and Sutherland 2013) | Global   |
| $A_T$   | L06  | SSS, SST                  | (Lee et al. 2006)               | Global   |
| $A_T$   | S13  | SSS, SST, DO,<br>Si, P    | (Sasse et al., 2013)            | Global   |
| $A_T$   | S13g | SST, SSS, DO,<br>Si, P    | (Sasse et al., 2013)            | Global   |
| $A_T$   |      | SSS                       | (Lefèvre et al. 2010)           | APR      |
| $A_T$   |      | SSS                       | (Cai et al. 2010)               | GCR, APR |
| $C_T$   | L00  | SSS, SST, N               | (Lee et al. 2000)               | Global   |
| $C_T$   | S13  | SST, SSS, DO, N,<br>Si, P | (Sasse et al., 2013)            | Global   |
| $C_T$   | S13g | SST, SSS, DO, N,<br>Si, P | (Sasse et al., 2013)            | Global   |
| $C_T$   |      | SSS                       | (Lefèvre et al. 2010)           | APR      |
| $C_T$   |      | SSS                       | (Bonou et al. 2016)             | APR      |

730

731

732

733 Table 2: Datasets used as inputs to the empirical algorithms. SSS = sea surface salinity, SST  
 734 = sea surface temperature, DO = dissolved oxygen.

|     | Type      | Name            | Time period | References            |
|-----|-----------|-----------------|-------------|-----------------------|
| SSS | Satellite | SMOS (CATDS v2) | 2010 - 2014 | (Reul and Team 2011)  |
| SSS | Satellite | Aquarius        | 2011 - 2014 | (Le Vine et al. 2014) |



|                           |             |             |             |   |
|---------------------------|-------------|-------------|-------------|---|
| SST                       | Satellite   | ESA SST CCI | 1992 - 2010 | (Merchant et al. 2012)  |
| SSS, SST                  | Re-analysis | CORA v4.0   | 1990 - 2012 | (Cabanes et al. 2013)   |
| SSS, SST,<br>DO, N, P, Si | Climatology | WOA         | 1970 - 2012 | (Garcia et al. 2014a;<br>Garcia et al. 2014b;<br>Locarnini et al. 2013;<br>Zweng et al. 2013) |

735

736

737 Table 3: *In situ* carbonate chemistry datasets used for evaluating the outputs. All datasets for  
738 each variable were combined into one dataset that was averaged monthly on a 1°x1° grid.  
739 The Bhadury et al. coastal data are from a sampling station located on the coast of India at  
740 21° 40' 40.6" N, 88° 9' 19.2"E, shown in Figure 1 of Choudhury et al. (2015) (Station 3).  
741 The Findlay et al. research cruise data are from cruises off the Svalbard and Greenland  
742 coasts, 78° 53' -59' N, 11° 42' -12° 27' E and 70° 14-49' N, 22° 4-32'W respectively.

|                                 | Dataset name                   | Time period | References                    |
|---------------------------------|--------------------------------|-------------|-------------------------------|
| A <sub>T</sub> , C <sub>T</sub> | GLODAPv2                       | 1970 – 2013 | (Olsen et al. 2016)           |
| A <sub>T</sub> , C <sub>T</sub> | OWS Mike                       | 2001 - 2007 | (Findlay et al. 2008)         |
| A <sub>T</sub>                  | Bhadury et al. coastal data    | 2014        | (Choudhury et al. 2015)       |
| A <sub>T</sub> , C <sub>T</sub> | Findlay et al. research cruise | 2012 – 2014 | [Findlay <i>pers. comm.</i> ] |

743

744

745 Table 4: Coverage, RMSDe and bias of the lowest RMSDe output for each SSS source in  
746 each region and carbonate parameter. Note that coverage is compared to all possible  
747 matchups, so recent SSS sources such as satellites have relatively low coverage.

| SSS INPUT                               | COVERAGE (%) | RMSDe (μmol kg <sup>-1</sup> ) | BIAS (μmol kg <sup>-1</sup> ) |
|---|--------------|--------------------------------|-------------------------------|
| <b>GLOBAL A<sub>T</sub> (N=6019)</b>    |              |                                |                               |
| <b><i>In situ</i> SD for comparison</b> |              | <b>81</b>                      |                               |
| SSS_CORA                                | 88           | 17                             | 0                             |
| SSS_AQUARIUS                            | 4            | 17                             | 3                             |
| SSS_SMOS                                | 6            | 17                             | -5                            |
| HG2                                     | 100          | 32                             | -17                           |
| SSS_CORA_CLIM                           | 96           | 17                             | -2                            |
| SSS_WOA_CLIM                            | 96           | 17                             | 0                             |

|  |     |            |     |
|--|-----|------------|-----|
| SSS_SMOS_CLIM                              | 94  | 18         | 1   |
| SSS_AQUARIUS_CLIM                          | 93  | 18         | -5  |
| HG2_CLIM                                   | 100 | 31         | -16 |
| <b>G CARIB A<sub>T</sub> (N=55)</b>        |     |            |     |
| <b><i>In situ SD for comparison</i></b>    |     | <b>13</b>  |     |
| SSS_CORA                                   | 96  | 17         | 3   |
| SSS_AQUARIUS                               | 13  | 19         | -4  |
| SSS_SMOS                                   | 13  | 20         | -4  |
| HG2  | 100 | 50         | 50  |
| SSS_CORA_CLIM                              | 100 | 17         | -4  |
| SSS_WOA_CLIM                               | 100 | 17         | 3   |
| SSS_SMOS_CLIM                              | 100 | 17         | 3   |
| SSS_AQUARIUS_CLIM                          | 100 | 19         | 2   |
| HG2_CLIM                                   | 100 | 48         | 50  |
| <b>AMAZON A<sub>T</sub> (N=108)</b>        |     |            |     |
| <b><i>In situ SD for comparison</i></b>    |     | <b>68</b>  |     |
| SSS_SMOS                                   | 31  | 58         | 1   |
| SSS_AQUARIUS                               | 12  | 58         | 17  |
| SSS_CORA                                   | 78  | 59         | 10  |
| HG2  | 100 | 75         | 43  |
| SSS_CORA_CLIM                              | 100 | 57         | -1  |
| SSS_SMOS_CLIM                              | 100 | 59         | -2  |
| SSS_AQUARIUS_CLIM                          | 100 | 60         | 1   |
| SSS_WOA_CLIM                               | 100 | 60         | -6  |
| HG2_CLIM                                   | 100 | 73         | 41  |
| <b>AMAZON S&lt;35 A<sub>T</sub> (N=15)</b> |     |            |     |
| <b><i>In situ SD for comparison</i></b>    |     | <b>115</b> |     |
| SSS_SMOS                                   | 20  | 132        | 124 |
| SSS_CORA                                   | 20  | 132        | 125 |
| SSS_AQUARIUS                               | 87  | 132        | 26  |
| HG2  | 100 | 172        | 128 |
| SSS_CORA_CLIM                              | 100 | 132        | 25  |
| SSS_AQUARIUS_CLIM                          | 100 | 133        | -19 |
| SSS_WOA_CLIM                               | 100 | 135        | 24  |
| SSS_SMOS_CLIM                              | 100 | 136        | 20  |
| HG2_CLIM                                   | 100 | 166        | 121 |
| <b>BENGAL A<sub>T</sub> (N=23)</b>         |     |            |     |
| <b><i>In situ SD for comparison</i></b>    |     | <b>16</b>  |     |
| SSS_CORA                                   | 96  | 11         | -3  |
| HG2  | 100 | 52         | 77  |
| SSS_CORA_CLIM                              | 100 | 10         | -3  |
| SSS_SMOS_CLIM                              | 100 | 10         | 3   |
| SSS_WOA_CLIM                               | 100 | 11         | 5   |
| SSS_AQUARIUS_CLIM                          | 100 | 11         | -2  |
| HG2_CLIM                                   | 100 | 55         | 83  |
| <b>GLOBAL C<sub>T</sub> (N=6689)</b>       |     |            |     |
| <b><i>In situ SD for comparison</i></b>    |     | <b>69</b>  |     |
| SSS_CORA                                   | 90  | 30         | -9  |
| SSS_SMOS                                   | 6   | 30         | -13 |
| SSS_AQUARIUS                               | 3   | 30         | 23  |
| HG2  | 100 | 33         | -13 |
| SSS_WOA_CLIM                               | 99  | 29         | -8  |

|  |     |           |     |
|--|-----|-----------|-----|
| SSS_CORA_CLIM                              | 99  | 29        | -8  |
| SSS_AQUARIUS_CLIM                          | 96  | 30        | 21  |
| SSS_SMOS_CLIM                              | 97  | 31        | 22  |
| HG2_CLIM                                   | 100 | 34        | -17 |
| <b>G CARIB C<sub>T</sub> (N=53)</b>        |     |           |     |
| <b><i>In situ SD for comparison</i></b>    |     | <b>18</b> |     |
| SSS_CORA                                   | 96  | 19        | 14  |
| SSS_SMOS                                   | 13  | 19        | 3   |
| SSS_AQUARIUS                               | 13  | 19        | 4   |
| HG2  | 100 | 42        | 52  |
| SSS_WOA_CLIM                               | 100 | 19        | 9   |
| SSS_CORA_CLIM                              | 100 | 19        | 10  |
| SSS_SMOS_CLIM                              | 100 | 19        | 10  |
| SSS_AQUARIUS_CLIM                          | 100 | 19        | 8   |
| HG2_CLIM                                   | 100 | 36        | 45  |
| <b>AMAZON C<sub>T</sub> (N=155)</b>        |     |           |     |
| <b><i>In situ SD for comparison</i></b>    |     | <b>53</b> |     |
| SSS_CORA                                   | 85  | 45        | 3   |
| SSS_SMOS                                   | 21  | 45        | 3   |
| SSS_AQUARIUS                               | 8   | 48        | 0   |
| HG2  | 100 | 57        | 33  |
| SSS_CORA_CLIM                              | 100 | 45        | 0   |
| SSS_SMOS_CLIM                              | 100 | 45        | 0   |
| SSS_WOA_CLIM                               | 100 | 45        | -2  |
| SSS_AQUARIUS_CLIM                          | 100 | 46        | -1  |
| HG2_CLIM                                   | 100 | 53        | 30  |
| <b>AMAZON S&lt;35 C<sub>T</sub> (N=17)</b> |     |           |     |
| <b><i>In situ SD for comparison</i></b>    |     | <b>96</b> |     |
| SSS_SMOS                                   | 18  | 109       | 100 |
| SSS_AQUARIUS                               | 18  | 109       | 108 |
| SSS_CORA                                   | 94  | 109       | 45  |
| HG2  | 100 | 132       | 118 |
| SSS_SMOS_CLIM                              | 100 | 109       | 3   |
| SSS_CORA_CLIM                              | 100 | 109       | 44  |
| SSS_AQUARIUS_CLIM                          | 100 | 111       | 21  |
| SSS_WOA_CLIM                               | 100 | 111       | 45  |
| HG2_CLIM                                   | 100 | 125       | 108 |
| <b>BENGAL C<sub>T</sub> (N=24)</b>         |     |           |     |
| <b><i>In situ SD for comparison</i></b>    |     | <b>10</b> |     |
| SSS_CORA                                   | 96  | 19        | 16  |
| HG2  | 100 | 36        | 51  |
| SSS_CORA_CLIM                              | 100 | 18        | -12 |
| SSS_WOA_CLIM                               | 100 | 18        | -11 |
| SSS_SMOS_CLIM                              | 100 | 19        | -14 |
| SSS_AQUARIUS_CLIM                          | 100 | 20        | -17 |
| HG2_CLIM                                   | 100 | 34        | 48  |

748

749 Table 5: Selected importances of exclusions for each carbonate parameter and region. A

750 source of SSS or SST can be monthly (M), climatological (C) or all (no prefix). Importances

751 are the percentage increase in RMSDe as a result of excluding all the listed inputs or

752 algorithms. Only exclusions mentioned in the text are listed here, more complete lists can be  
 753 found in (Land et al., 2019).

| EXCLUSIONS                            | IMPORTANCE (%) | NOTES                          |
|---------------------------------------|----------------|--------------------------------|
| <b>(GLOBAL A<sub>T</sub>)</b>         |                |                                |
| TS13,L06,S13g                         | 3.1            | Only leaves S13,HG2            |
| TS13,L06,S13g,S13                     | 85             | Only leaves HG2                |
| CORA,M SMOS,M Aquarius,WOA SSS        | 3.0            | Only leaves C SMOS,C Aquarius  |
| CORA,SMOS,M Aquarius,WOA SSS          | 4.1            | Only leaves C Aquarius         |
| <b>(G CARIB A<sub>T</sub>)</b>        |                |                                |
| CORA,WOA,C SMOS SSS                   | 13             | Only leaves M SMOS,Aquarius    |
| TS13,L06,S13g,Cai10                   | 2.9            | Only leaves S13,HG2            |
| TS13,L06,S13g,Cai10,S13               | 286            | Only leaves HG2                |
| CORA,WOA,C Aquarius,C SMOS SSS        | 16             | Only leaves M SMOS,M Aquarius  |
| CORA,WOA,Aquarius,C SMOS SSS          | 18             | Only leaves M SMOS             |
| <b>(AMAZON A<sub>T</sub>)</b>         |                |                                |
| TS13,L06,S13,S13g                     | 2.6            |                                |
| TS13,L06,S13,S13g,Cai10               | 4.4            | Only leaves Lefevre10,HG2      |
| SMOS,CORA,M Aquarius SSS              | 4.0            | Only leaves C Aquarius,WOA SSS |
| TS13,L06,S13,S13g,Cai10,Lefevre10     | 26             | Only leaves HG2                |
| SMOS,CORA,Aquarius SSS                | 5.1            | Only leaves WOA SSS            |
| <b>(AMAZON S&lt;35 A<sub>T</sub>)</b> |                |                                |
| M SMOS,M Aquarius SSS,M CCI SST       | 2.5            | All monthly satellite data     |
| M SMOS,Aquarius SSS,M CCI SST         | 3.2            |                                |
| SMOS,Aquarius SSS,M CCI SST           | 4.6            |                                |
| M SMOS,Aquarius,CORA SSS              | 2.9            |                                |
| TS13,L06,S13,S13g,Cai10,Lefevre10     | 26             | Only leaves HG2                |
| <b>(BENGAL A<sub>T</sub>)</b>         |                |                                |
| C CORA SSS                            | 2.2            |                                |
| C CORA,C SMOS SSS                     | 5.1            |                                |
| C CORA,C SMOS,WOA SSS                 | 6.4            | Only leaves M CORA,C Aquarius  |
| TS13,L06,S13                          | 3.7            | Only leaves S13g,HG2           |
| TS13,L06,S13,S13g                     | 517            | Only leaves HG2                |
| CORA,C SMOS,WOA SSS                   | 8.1            | Only leaves C Aquarius         |
| <b>(GLOBAL C<sub>T</sub>)</b>         |                |                                |
| L00                                   | 3.6            |                                |
| L00,S13g                              | 5.3            |                                |
| L00,S13g,S13                          | 14             | Only leaves HG2                |
| CORA,WOA,M SMOS SSS                   | 3.6            |                                |
| CORA,WOA,M SMOS,M Aquarius SSS        | 4.4            | Only leaves C SMOS,C Aquarius  |
| CORA,WOA,Aquarius,M SMOS SSS          | 7.7            | Only leaves C SMOS             |
| <b>(G CARIB C<sub>T</sub>)</b>        |                |                                |
| L00,S13                               | 73             | Only leaves S13g and HG2       |
| L00,S13,S13g                          | 90             | Only leaves HG2                |
| SMOS,CORA,WOA,M Aquarius SSS          | 3.9            | Only leaves C Aquarius         |
| <b>(AMAZON C<sub>T</sub>)</b>         |                |                                |
| L00,S13,Bonou16,Lefevre10             | 2.1            | Only leaves S13g and HG2       |
| L00,S13,Bonou16,Lefevre10,S13g        | 19             | Only leaves HG2                |
| SMOS,CORA,WOA SSS                     | 3.6            | Only leaves Aquarius           |
| SMOS,CORA,C Aquarius,WOA SSS          | 7.0            | Only leaves M Aquarius         |
| <b>(AMAZON S&lt;35 C<sub>T</sub>)</b> |                |                                |
| L00,S13,Bonou16,Lefevre10             | 2.2            | Only leaves S13g and HG2       |
| L00,S13,Bonou16,Lefevre10,S13g        | 15             | Only leaves HG2                |

|                                  |     |                          |
|----------------------------------|-----|--------------------------|
| SMOS,Aquarius SSS,M CCI SST      | 2.6 | Only leaves CORA,WOA SSS |
| SMOS,Aquarius,CORA SSS,M CCI SST | 4.9 | Only leaves WOA SSS      |
| <b>(BENGAL Cr)</b>               |     |                          |
| S13                              | 2.1 |                          |
| S13,S13g                         | 9.9 |                          |
| C CORA,WOA SSS                   | 2.1 |                          |
| L00,S13,S13g                     | 83  | Only leaves HG2          |
| CORA,WOA SSS                     | 3.6 |                          |
| CORA,C SMOS,WOA SSS              | 5.9 |                          |

754

755 Table 6: Testing the sensitivity of the output uncertainties to that of the satellite remote  
756 sensing input data uncertainties using all global  $A_T$  algorithms (TS13, Lee06, Lee00, S13 and  
757 S13g) and exemplar uncertainties from the literature (for SST, Merchant *et al.*, (2014) gives  
758  $\pm 0.15^\circ\text{C}$ ; for SSS, Boutin *et al.*, (2018) gives  $\pm 0.2$ ). The output uncertainties are given as a  
759 percentage of a global value of  $2000 \mu\text{mol kg}^{-1}$  and the quoted values are the maximum open-  
760 ocean values calculated for all data within latitudes  $< \pm 60^\circ$ .

| Algorithm | Uncertainty in $A_T$ due to SSS (%) | Uncertainty in $A_T$ due to SST (%) |
|-----------|-------------------------------------|-------------------------------------|
| TS13      | $< \pm 0.8$                         | N/A                                 |
| Lee06     | $< \pm 0.7$                         | $< \pm 0.2$                         |
| Lee00     | $< \pm 0.9$                         | $< \pm 0.2$                         |
| S13       | $< \pm 0.6$                         | $< \pm 0.1$                         |
| S13g      | $< \pm 0.6$                         | $< \pm 0.1$                         |

761

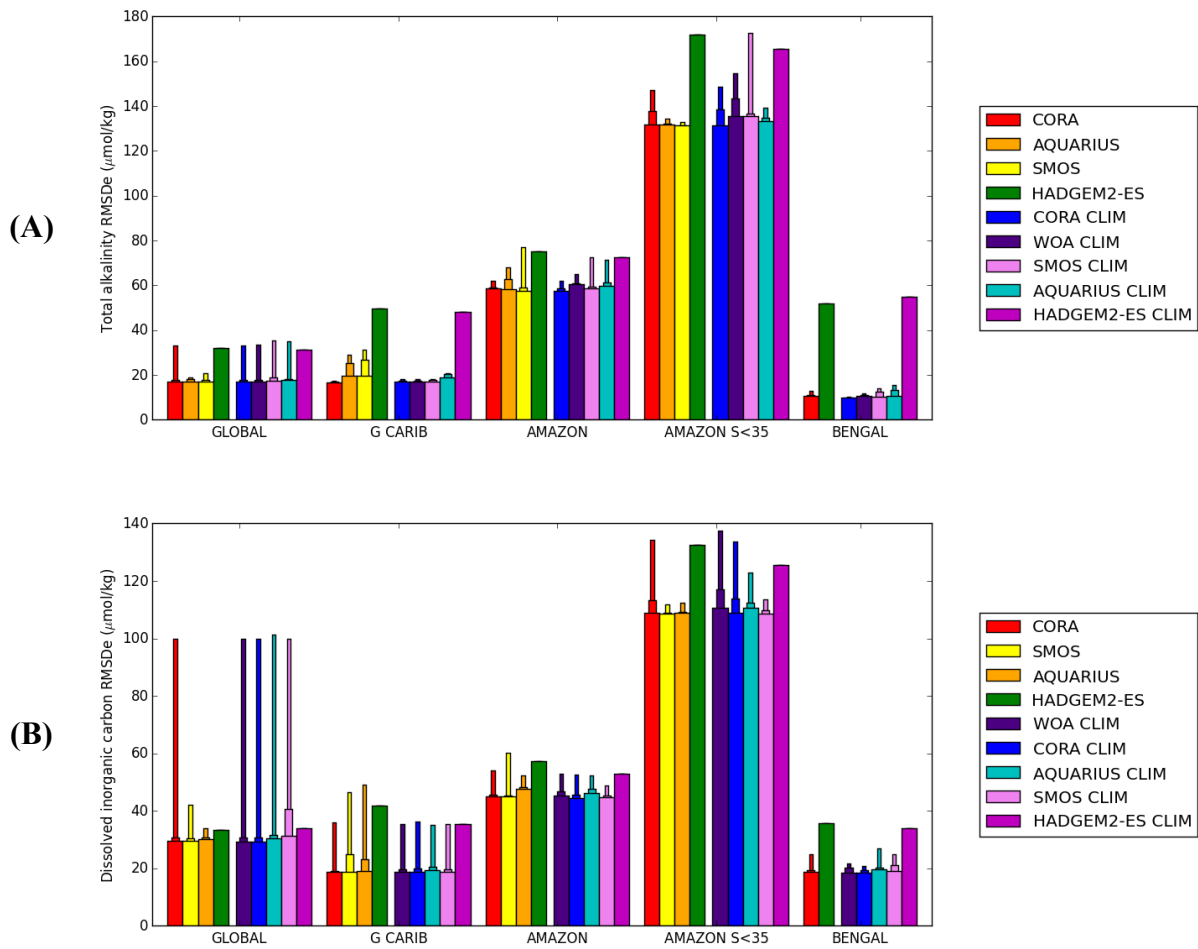


Figure 1: Estimated regional weighted RMSD (RMSDe) for each SSS source. Data are grouped by region, then by whether the input data are climatological (left group) or monthly (right group), then by SSS source. All regional outputs using a given SSS source are considered, and the wide bar shows the lowest RMSDe of these, the half-width bar shows the median RMSDe and the thin bar shows the highest RMSDe. SSS sources in each group are shown in order of global lowest RMSDe. (A)  $A_T$  results; (B)  $C_T$  results.

763

764

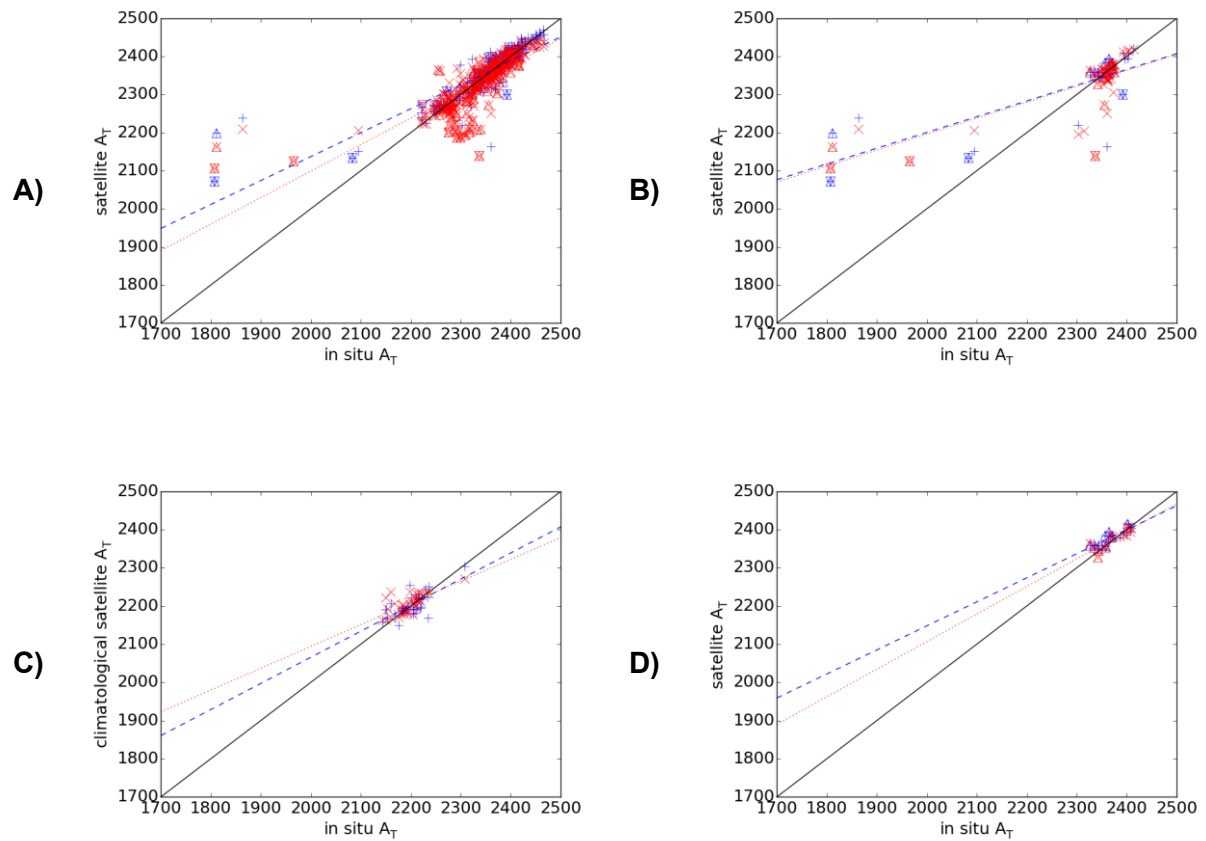


Figure 2: Comparison of  $A_T$  estimated using monthly satellite SSS with *in situ* measured  $A_T$ . (A) global; (B) Amazon plume; (C) Bay of Bengal using climatological satellite SSS; (D) Greater Caribbean. The algorithm is (Takahashi et al. 2013) with climatological WOA nitrate. Red crosses use SMOS SSS, blue plusses use Aquarius. Points with down-pointing triangles have depth less than 500 m, those with up-pointing triangles are less than 300 km from the nearest coast. Regressions use all data.

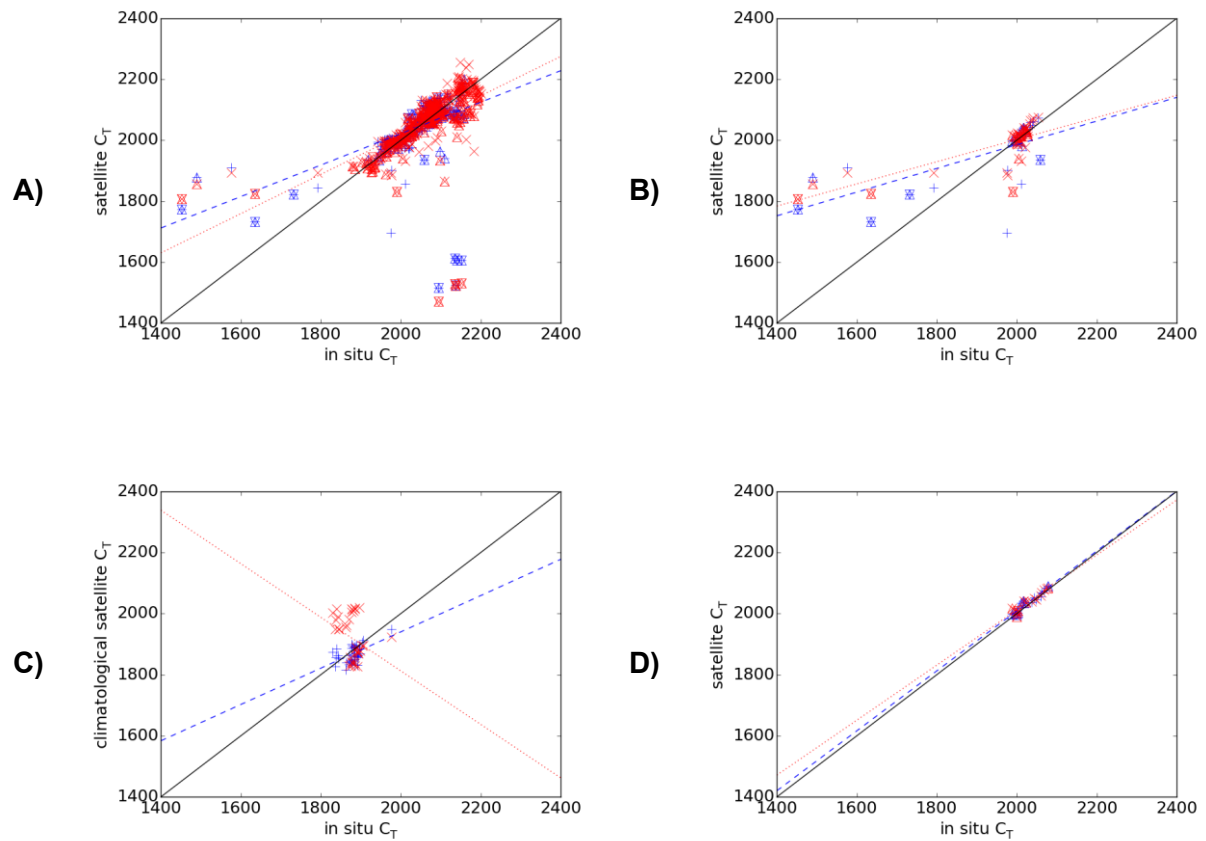


Figure 3: Comparison of  $C_T$  estimated using monthly satellite SSS with in situ measured  $C_T$ . (A) global; (B) Amazon plume; (C) Bay of Bengal using climatological satellite SSS; (D) Greater Caribbean. The algorithm is (Lee et al. 2000) with climatological WOA SST and nitrate. Red crosses use SMOS SSS, blue plusses use Aquarius. Points with down-pointing triangles have depth less than 500 m, those with up-pointing triangles are less than 300 km from the nearest coast. Regressions use all data.

766

767



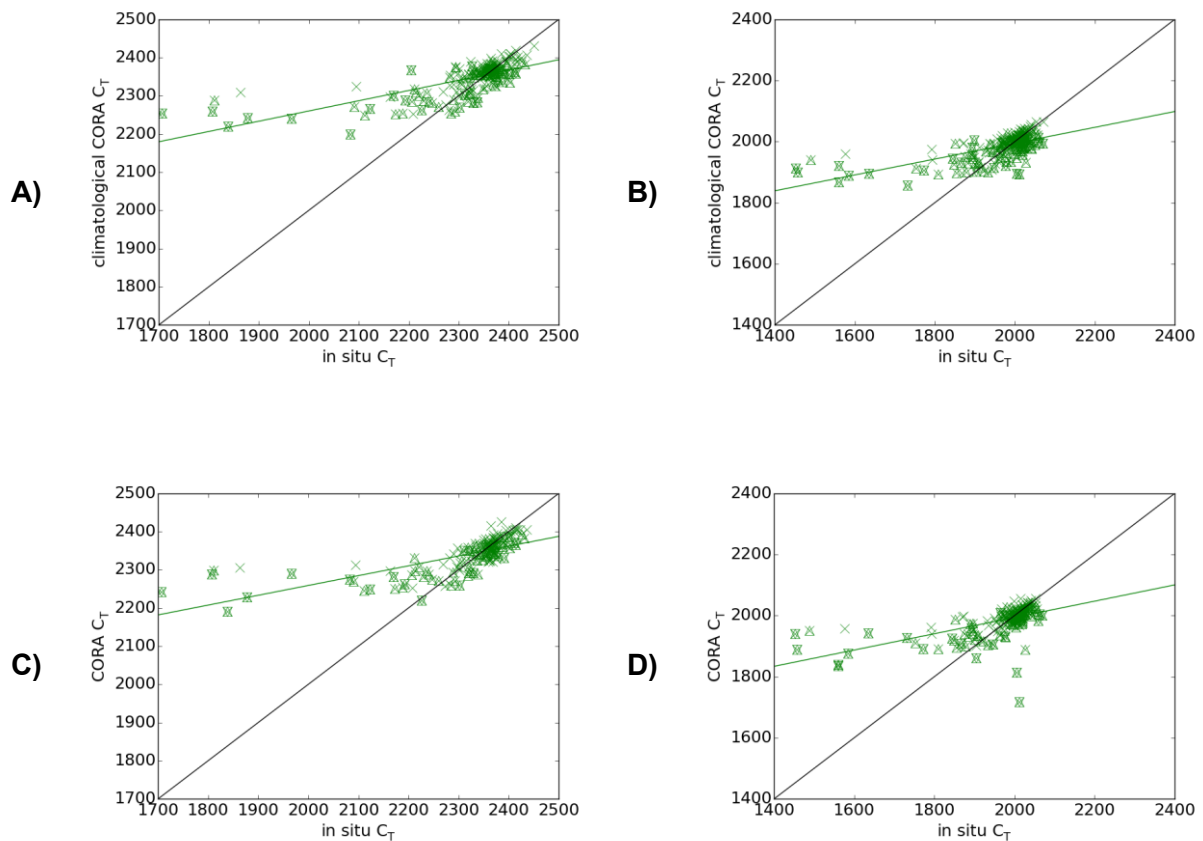


Figure 4: Comparison of  $A_T$  and  $C_T$  estimated from CORA (interpolated *in situ*) SSS with *in situ* measured values in the Amazon plume. (A)  $A_T$  comparison using climatological CORA SSS; (B)  $C_T$  comparison using climatological CORA SSS; (C)  $A_T$  comparison using monthly CORA SSS; (D)  $C_T$  comparison using monthly CORA SSS. The  $A_T$  algorithm is (Takahashi et al. 2013) with climatological WOA nitrate, and the  $C_T$  algorithm is (Lee et al. 2000) with climatological CORA SST and climatological WOA nitrate. Points with down-pointing triangles have depth less than 500 m, those with up-pointing triangles are less than 300 km from the nearest coast. Regressions use all data.

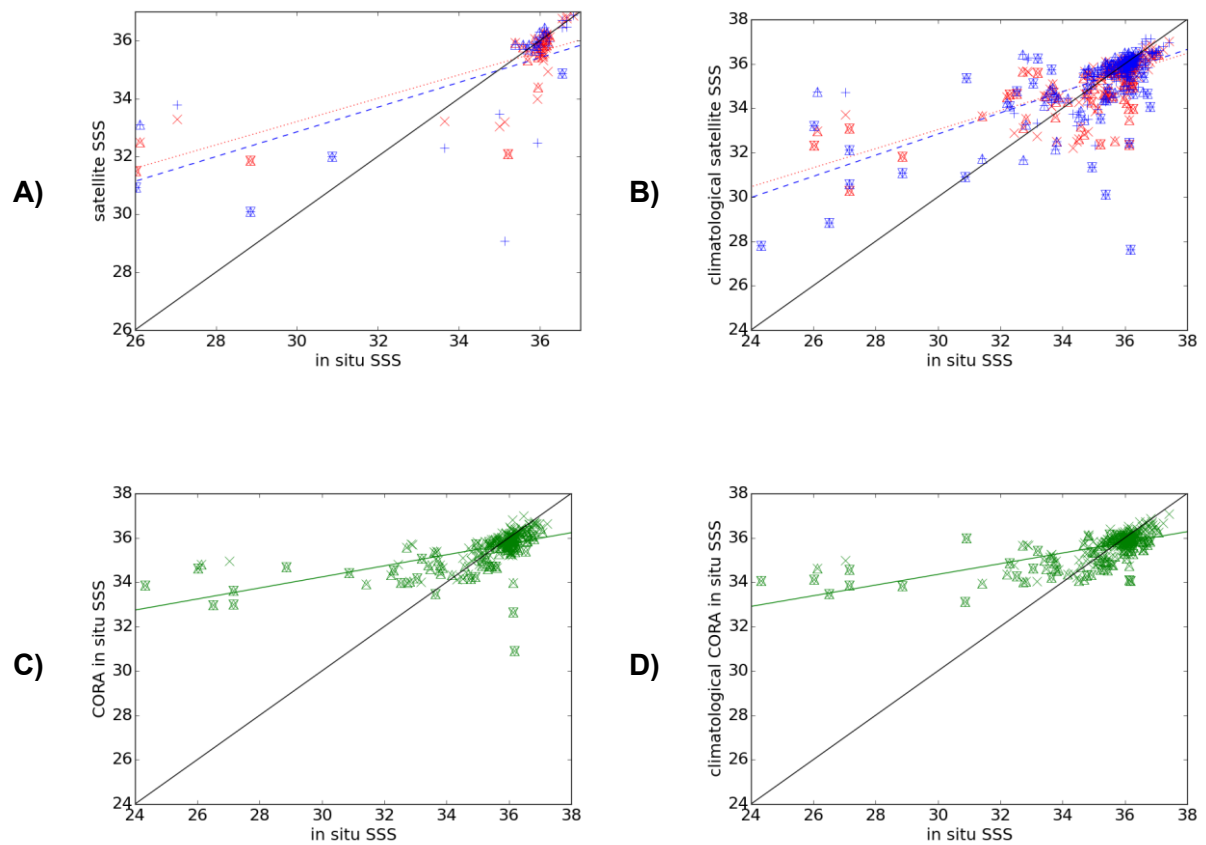


Figure 5: Comparison of satellite and CORA SSS with *in situ* measured SSS in the Amazon plume. (A) monthly SMOS (red crosses) and Aquarius (blue pluses); (B) climatological SMOS and Aquarius; (C) monthly CORA; (D) climatological CORA. Points with down-pointing triangles have depth less than 500 m, those with up-pointing triangles are less than 300 km from the nearest coast. Regressions use all data.

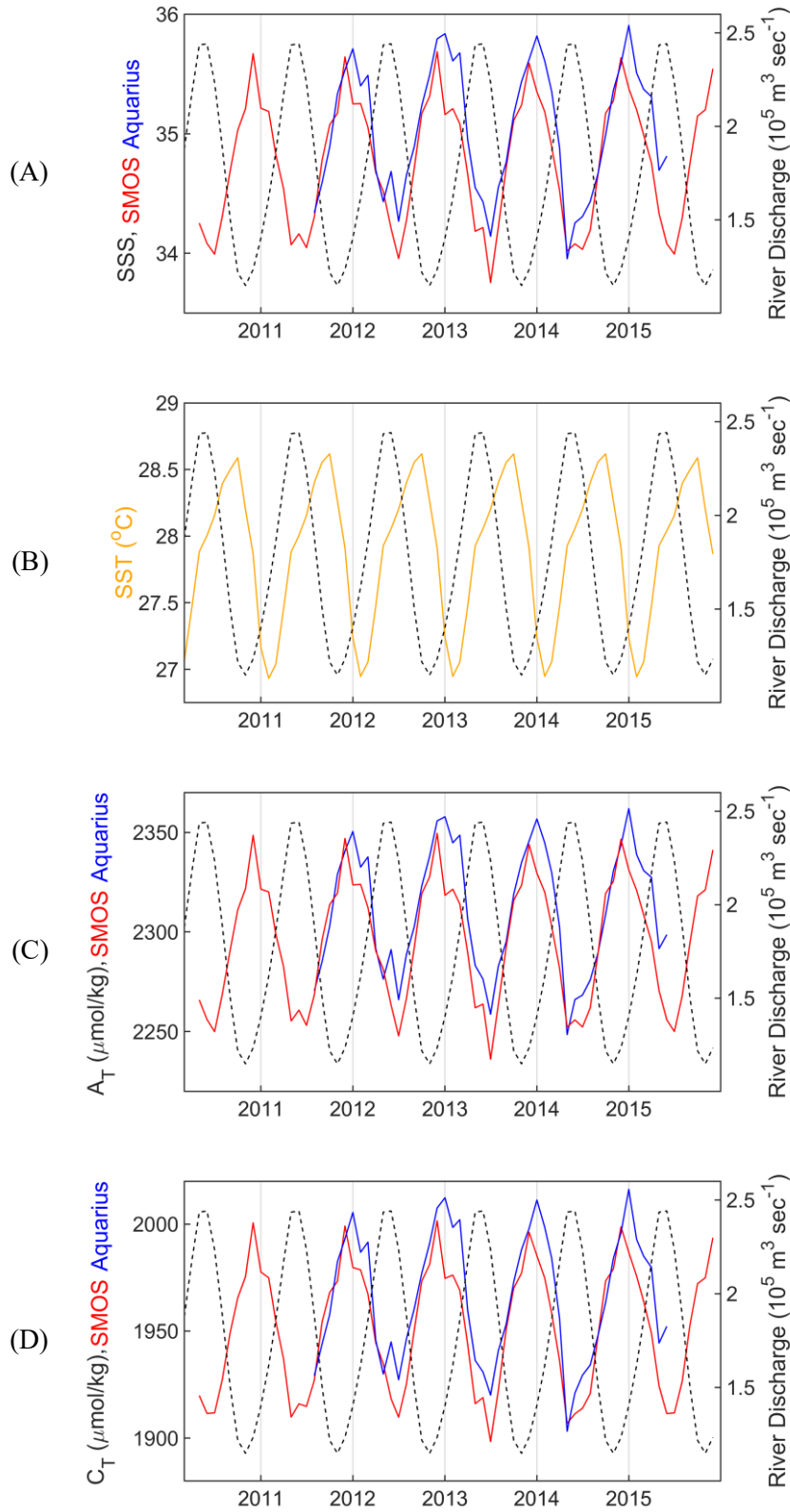


Figure 6: Time series of Amazon plume discharge and averaged satellite observations between 2010 and 2016. Monthly observations were average over the area  $0^{\circ}$ - $15^{\circ}$  N,

45°-62° W. Dashed black lines are climatological discharge at the Obidos gauge, red use SMOS SSS and blue use Aquarius SSS. In months containing both SMOS and Aquarius data, only cells with valid data in both are used. (A) monthly SMOS and Aquarius SSS; (B) climatological CORA (orange) SST; (C)  $A_T$  using the TS13 algorithm and WOA nitrate, with monthly SMOS and Aquarius SSS; (D)  $C_T$  using the L00 algorithm, CORA SST climatology and WOA nitrate, with monthly SMOS and Aquarius SSS.

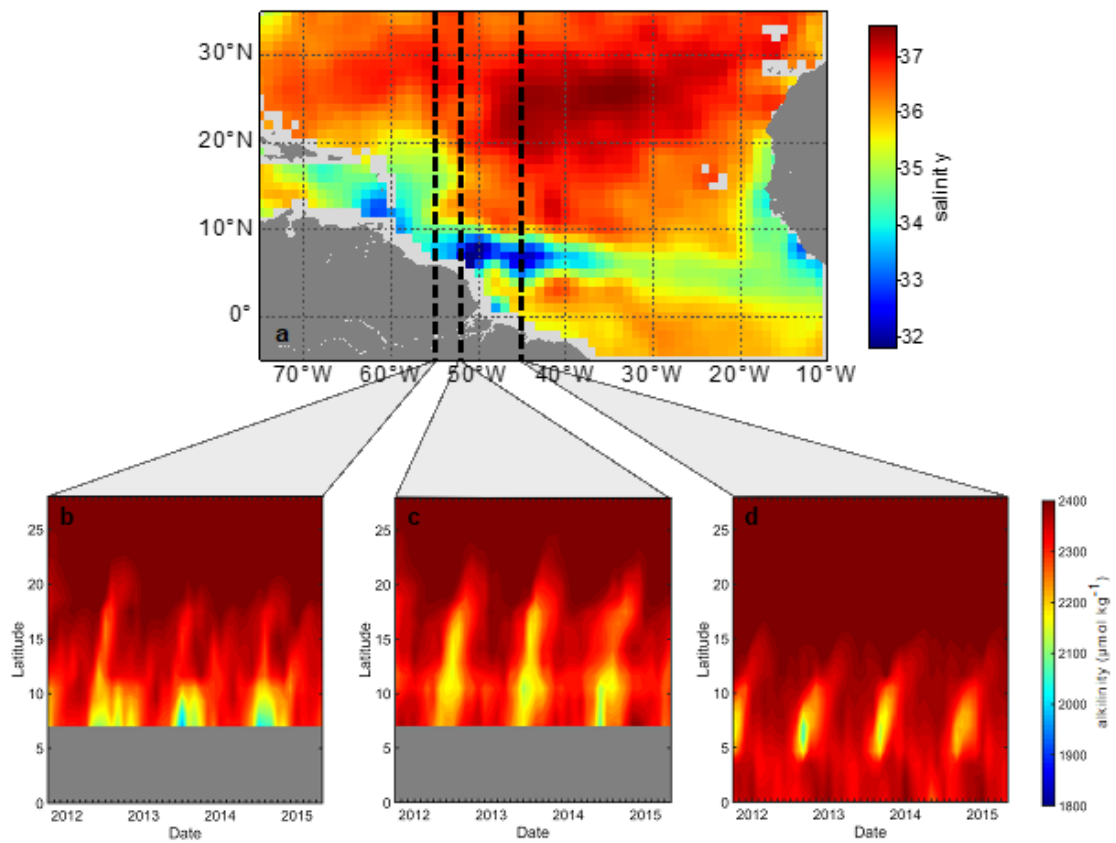


Figure 7: Aquarius derived synoptic scale observations of  $A_T$  in  $\mu\text{mol kg}^{-1}$  for the Amazon Plume between August 2011 and June 2015 using the TS13 algorithm and WOA nitrate, with monthly SMOS and Aquarius SSS: (a)  $A_T$  in August 2011 showing the bifurcation of the plume; (b) Hovmöller time series plot for  $55^\circ\text{W}$ ; (c) Hovmöller time series plot for  $52^\circ\text{W}$  and (d) Hovmöller time series plot for  $45^\circ\text{W}$ .

774

775

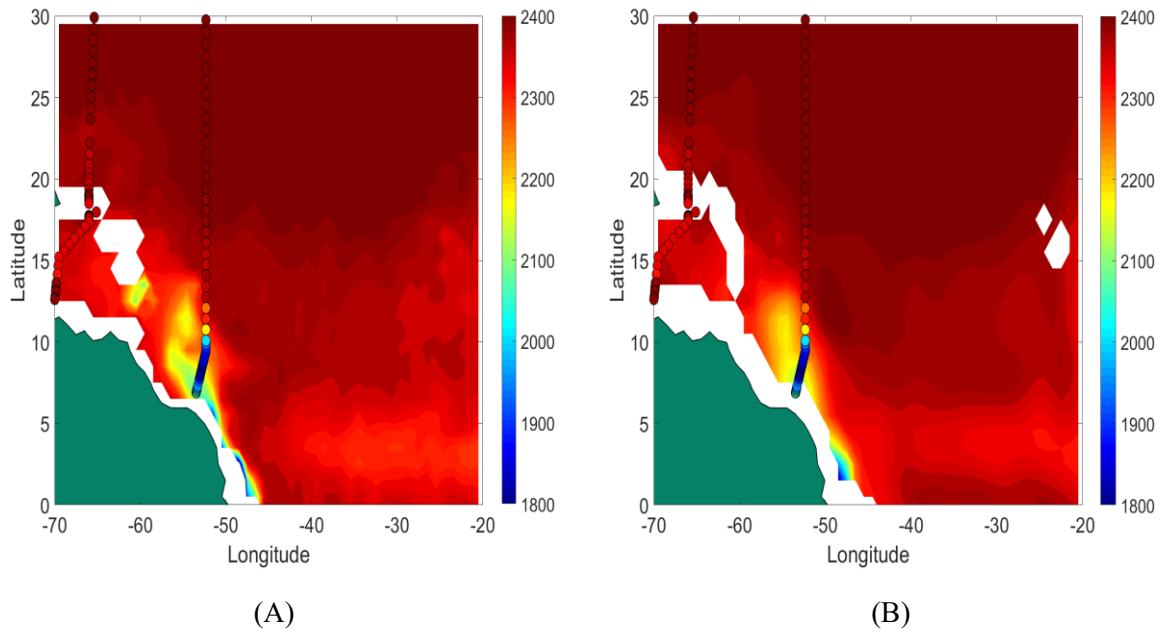
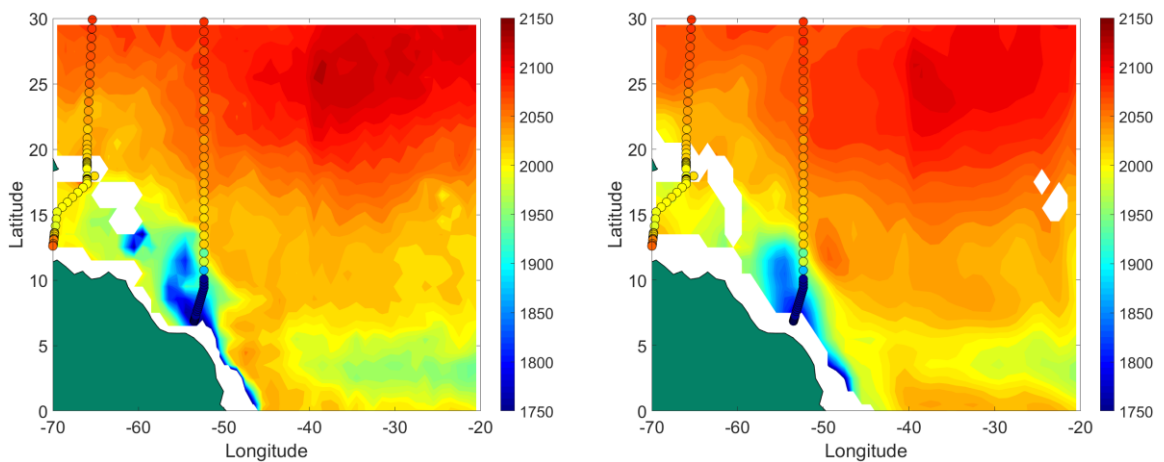


Figure 8: Synoptic scale Aquarius (A) and SMOS (B) derived  $A_T$  in  $\mu\text{mol kg}^{-1}$  for April 2012 using the TS13 algorithm and WOA nitrate, with monthly SMOS and Aquarius SSS. *In situ* observations collected in April and May 2012 from the GLODAPv2 dataset are overlaid as circles. The May 2012 *in situ* observations are all within the offshore region (latitude  $>20^\circ$  N).

776



777

Figure 9: Synoptic scale Aquarius (A) and SMOS (B) derived  $C_T$  in  $\mu\text{mol kg}^{-1}$  for April 2012

using the L00 algorithm, CORA SST climatology and WOA nitrate, with monthly SMOS and Aquarius SSS. *In situ* observations collected in April and May 2012 from the GLODAPv2 dataset are overlaid as circles. The May 2012 *in situ* observations are all within the offshore region (latitude >20° N).

778

779 **Copyrighted material permission**

780 None required

781

782 **Supporting information/non-print material**

783 Supporting Information: Land et al., (2019) and landetal-SupportingInformation.docx

784

785 **References**

786 Akhand, A., Chanda, A., Dutta, S. Characterizing air-sea CO<sub>2</sub> exchange dynamics during  
787 winter in the coastal water off the Hugli-Matla estuarine system in the northern Bay  
788 of Bengal, India. *Journal of Oceanography* **69**, 687-697 (2013).

789 Akhand, A. *et al.* Potential CO<sub>2</sub> Emission Due to Loss of Above Ground Biomass from the  
790 Indian Sundarban Mangroves During the Last Four Decades. *Journal of the Indian*  
791 *Society of Remote Sensing*, **45**(1), 147-154 (2017).

792 Bates, N. R. *et al.* Detecting anthropogenic carbon dioxide uptake and ocean acidification in  
793 the North Atlantic Ocean. *Biogeosciences* **9**, 2509-2522, doi:10.5194/bg-9-2509-2012  
794 (2012).

795 BIPM, (2008) *Evaluation of measurement data – Guide to the expression of uncertainty in*  
796 *measurement*, JCGM 100:2008.

797 Bockmon, E. E., Dickson, A. G. An inter-laboratory comparison assessing the quality of  
798 seawater carbon dioxide measurements. *Marine Chemistry* **171**, 36-43,  
799 doi:10.1016/j.marchem.2015.02.002 (2015).

800 Bonou, F. K., Noriega, C., Lefèvre, N., Araujo, M. Distribution of CO<sub>2</sub> parameters in the  
801 Western Tropical Atlantic Ocean. *Dynamics of Atmospheres and Oceans* **73**, 47-60,  
802 doi:http://dx.doi.org/10.1016/j.dynatmoce.2015.12.001 (2016).

803 Boutin, J., Martin, N., Reverdin, G., Yin, X., Gaillard, F. Sea surface freshening inferred  
804 from SMOS and ARGO salinity: Impact of rain. *Ocean Science* **9**, 183 (2013).

805 Boutin, J. *et al.* Satellite and in situ salinity: understanding near-surface stratification and  
806 subfootprint variability. *Bulletin of the American Meteorological Society* **97**, 1391-  
807 1407 (2016).

808 Boutin, J., Vergrly, J. L., Marchand, S., D'Amico, F., Hasson, A., Kolodziejczyk, N., Reul,  
809 N., Reverdin, G., Vialard, J., New SMOS Sea Surface Salinity with reduced  
810 systematic errors and improved variability, *Remote Sensing of Environment*, 214, 115-  
811 134, doi:10.1016/j.rse.2018.05.022 (2018).

812 Brix, H., Gruber, N., Keeling, C. D. Interannual variability of the upper ocean carbon cycle at  
813 station ALOHA near Hawaii. *Global Biogeochemical Cycles* **18**,  
814 doi:10.1029/2004GB002245 (2004).

815 Byrne, R. H. Measuring Ocean Acidification: New Technology for a New Era of Ocean  
816 Chemistry. *Environmental Science and Technology*, 48(10), 5352–5360 (2014).

817 Cabanes, C. *et al.* The CORA dataset: validation and diagnostics of in-situ ocean temperature  
818 and salinity measurements. *Ocean Science* **9**, 1-18, doi:10.5194/os-9-1-2013 (2013).

819 Cai, W.-J. *et al.* Alkalinity distribution in the western North Atlantic Ocean margins. *Journal*  
820 *of Geophysical Research: Oceans* **115**, n/a-n/a, doi:10.1029/2009JC005482 (2010).



821 Caldeira, K. and Wickett, M. E., Ocean model predictions of chemistry changes from carbon  
822 dioxide emissions to the atmosphere and ocean. *Journal of Geophysical Research-*  
823 *Oceans*, doi: 10.1029/2004JC002671 (2005).

824 Cooley, S. R., Coles, V. J., Subramaniam, A., Yager, P. L. Seasonal variations in the Amazon  
825 plume-related atmospheric carbon sink. *Global Biogeochemical Cycles* **21**, n/a-n/a,  
826 doi:10.1029/2006GB002831 (2007).

827 Chao, Y., Farrara, J. D., Schumann, G., Andreadis, K. M., Moller, D. Sea surface salinity  
828 variability in response to the Congo River discharge. *Continental Shelf Research* **99**,  
829 35-45 (2015).

830 Choudhury, A. K., Das, M., Philip, P., Bhadury, P. An assessment of the implications of  
831 seasonal precipitation and anthropogenic influences on a mangrove ecosystem using  
832 phytoplankton as proxies. *Estuaries and Coasts* **38**, 854-872 (2015).

833 Del Vecchio, R., Subramaniam, A. Influence of the Amazon River on the surface optical  
834 properties of the western tropical North Atlantic Ocean. *Journal of Geophysical*  
835 *Research: Oceans* **109** (2004).

836 Dickson, A. G., Sabine, C. L., Christian, J. R. Guide to best practices for ocean CO<sub>2</sub>  
837 measurements, PICES Special Publication. (North Pacific Marine Science  
838 Organization, 2007).

839 Drucker, R., Riser, S. C. Validation of Aquarius sea surface salinity with Argo: Analysis of  
840 error due to depth of measurement and vertical salinity stratification. *J. Geophys. Res.*  
841 *Oceans* **119**, 4626-4637 (2014).

842 Fine, R. A., Willey, D. A. Millero, F. J. Global variability and changes in ocean total  
843 alkalinity from Aquarius satellite data, *Geophysical Research Letters*, **44**, 261–267,  
844 doi:10.1002/2016GL071712 (2017).

845 Friis, K., Körtzinger, A., Wallace, D. W. R. The salinity normalization of marine inorganic  
846 carbon chemistry data. *Geophysical Research Letters* **30**, doi:10.1029/2002GL015898  
847 (2003).

848 Ganguly, D. *et al.* Coupled micrometeorological and biological processes on atmospheric  
849 CO<sub>2</sub> concentrations at the land–ocean boundary, NE coast of India. *Atmospheric*  
850 *Environment* **45**, 3903–3910 (2011).

851 Garcia, H. E. *et al.* World Ocean Atlas 2009, Volume 4: Nutrients (Phosphate, Nitrate,  
852 Silicate), NOAA Atlas NESDIS 71, edited by S. Levitus. *US Gov. Print. Off.*,  
853 *Washington, DC*, 398 pp (2010).

854 Gledhill, D. K., Wanninkhof, R., Millero, F. J., Eakin, M. Ocean acidification of the greater  
855 Caribbean region 1996–2006. *Journal of Geophysical research* **113**, C10031,  
856 doi:10/1029/2007JC004629 (2008).

857 Gledhill, D. K., Wanninkhof, R., Eakin, C. M. Observing ocean acidification from space.  
858 *Oceanography* **22** (2009).

859 International Hydrographic Organization. *Limits of oceans and seas, Special Publication 23*.  
860 3 edn, (International Hydrographic Organization, 1953).

861 Ibánhez, J. S. P., Araujo, M., Lefèvre, N. The overlooked tropical oceanic CO<sub>2</sub> sink.  
862 *Geophysical Research Letters* **43**, 3804-3812 (2016).

863 Jiang, Z. P., Tyrrell, T., Hydes, D. J., Dai, M., Hartman, S. E. Variability of alkalinity and the  
864 alkalinity-salinity relationship in the tropical and subtropical surface ocean. *Global*  
865 *Biogeochemical Cycles* **28**, 729-742 (2014).

866 Johnson, K.S., J.N. Plant, L.J. Coletti, H.W. Jannasch, C.M. Sakamoto, S.C. Riser, D.D.  
867 Swift, N.L. Williams, E. Boss, N. Haëntjens, L.D. Talley, J.L. Sarmiento. J.  
868 Biogeochemical sensor performance in the SOCCOM profiling float array,  
869 *Geophysical Research-Oceans*, 122, 6416–6436. doi: 10.1002/2017JC012838 (2017).

870 Jones, C. D. *et al.* The HadGEM2-ES implementation of CMIP5 centennial simulations.  
871 *Geoscientific Model Development* **4**, 543-570, doi:10.5194/gmd-4-543-2011 (2011).

872 Kroeker, K. J. *et al.* Impacts of ocean acidification on marine organisms: quantifying  
873 sensitivities and interaction with warming. *Glob Chang Biol* **19**, 1884-1896,  
874 doi:10.1111/gcb.12179 (2013).

875 Land, P. E. *et al.* Salinity from space unlocks satellite-based assessment of ocean  
876 acidification. *Environmental science & technology* **49**, 1987-1994,  
877 doi:10.102/es504849s (2015).

878 Land, P. E., Findlay, H. S., Shutler, J. D., Ashton, I. G. C., Grouazel, A., Girard-Arduin, F.,  
879 Reul, N., Piolle, J.-F., Chapron, B., Quilfen, Y., Bellerby, R. G. J., Bhadury, P.,  
880 Salisbury, J., Vandemark, D., Sabia, R., Results and analysis of oceanic total  
881 alkalinity and dissolved inorganic carbon estimated from space borne, interpolated in  
882 situ, climatological and Earth system model data. *PANGAEA*,  
883 doi:10.1594/PANGAEA.898115 (2019).

884 Lagerloef, G., Kao, H. Y., Meissner, T., Vazquez, J. Aquarius salinity validation analysis;  
885 data version 4.0. *Earth Space Res., Seattle, WA, USA* (2015).

886 Lee, K. *et al.* Global relationships of total alkalinity with salinity and temperature in surface  
887 waters of the world's oceans. *Geophysical Research Letters* **33** (2006).

888 Lee, K., Wanninkhof, R., Feely, R. A., Millero, F. J., Peng, T. H. Global relationships of total  
889 inorganic carbon with temperature and nitrate in surface seawater. *Global*  
890 *Biogeochemical Cycles* **14**, 979-994 (2000).

891 Lefèvre, N., Diverrès, D., Gallois, F. Origin of CO<sub>2</sub> undersaturation in the western tropical  
892 Atlantic. *Tellus B* **62**, 595-607, doi:10.1111/j.1600-0889.2010.00475.x (2010).

893 Lentz, S. J., Limeburner, R. The Amazon River Plume during AMASSEDS: Spatial  
894 characteristics and salinity variability. *Journal of Geophysical Research: Oceans* **100**,  
895 2355-2375 (1995).

896 Le Vine, D. M. *et al.* Aquarius: Status and recent results. *Radio Science* **49**, 709-720,  
897 doi:10.1002/2014RS005505 (2014).

898 Merchant, C. J. *et al.* A 20 year independent record of sea surface temperature for climate  
899 from Along-Track Scanning Radiometers. *Journal of Geophysical Research: Oceans*  
900 (1978–2012) **117** (2012).

901 Merchant, C. J. *et al.* Sea surface temperature datasets for climate applications from Phase 1  
902 of the European Space Agency Climate Change Initiative (SST CCI). *Geoscience*  
903 *Data Journal* **1**, 179-191 (2014).

904 Millero, F. J., Lee, K., Roche, M. Distribution of alkalinity in the surface waters of the major  
905 oceans. *Marine Chemistry* **60**, 111-130 (1998).

906 Olsen, A. *et al.* The Global Ocean Data Analysis Project version 2 (GLODAPv2) – an  
907 internally consistent data product for the world ocean. *Earth System Science Data* **8**,  
908 297-323, doi:10.5194/essd-8-297-2016 (2016).

909 Osterman, G.B., Elderling, A., Avis, C., Chafin, B., O’Dell, C.W., Frankenberg, C., Fisher,  
910 B.M., Mandrake, L., Wunch, D., & Granat, R. Orbiting Carbon Observatory-2 (OCO-  
911 2) data product user’s guide, operational L1 and L2 data versions 7 and 7R. *Jet*  
912 *Propulsion Laboratory, Pasadena, CA, USA* (2016).

913 Perry, G. D., Duffy, P. B., Miller, N. L. An extended data set of river discharges for  
914 validation of general circulation models. *Journal of Geophysical Research:*  
915 *Atmospheres* **101**, 21339-21349 (1996).

916 Raven, J. A., Caldeira, K., Elderfield, H., Hoegh-Guldberg, O., Liss, P. S., Riebesell, U., et

917 al. Ocean acidification due to increasing atmospheric carbon dioxide, *The Royal*  
918 *Society*, Policy document 12/05 (2005).

919 Reul, N. and Team, I. C.-C. *SMOS Level 3 and 4 Research products of the Centre*  
920 *d'Expertise Ifremer du CATDS -Algorithm Theoretical Background Document,*  
921 *IFREMER-CNES technical document 2015*, <<https://www.catds.fr/>> (2015).

922 Reul, N. *et al.* Overview of the first SMOS sea surface salinity products. Part I: Quality  
923 assessment for the second half of 2010. *IEEE Transactions on Geoscience and*  
924 *Remote Sensing* **50**, 1636-1647 (2012).

925 Reul, N. *et al.* Sea surface salinity observations from space with the SMOS satellite: A new  
926 means to monitor the marine branch of the water cycle. *Surveys in Geophysics* **35**,  
927 681 (2014).

928 Salisbury, J. *et al.* Spatial and temporal coherence between Amazon River discharge, salinity,  
929 and light absorption by colored organic carbon in western tropical Atlantic surface  
930 waters. *Journal of Geophysical Research: Oceans* **116** (2011).

931 Salisbury, J. *et al.* How Can Present and Future Satellite Missions Support Scientific Studies  
932 that Address Ocean Acidification? *Oceanography* **28**, 108-121,  
933 doi:10.5670/oceanog.2015.35 (2015).

934 Samanta, S., Dalai, T. K., Pattanaik, J. K., Rai, S. K., Mazumdar, A. Dissolved inorganic  
935 carbon (DIC) and its  $\delta^{13}\text{C}$  in the Ganga (Hooghly) River estuary, India: Evidence of  
936 DIC generation via organic carbon degradation and carbonate dissolution.  
937 *Geochimica et Cosmochimica Acta* **165**, 226-248 (2015).

938 Santana-Casiano, J. M., González-Dávila, M., Rueda, M. J., Llinás, O., González-Dávila, E.  
939 F. The interannual variability of oceanic CO<sub>2</sub> parameters in the northeast Atlantic  
940 subtropical gyre at the ESTOC site. *Global Biogeochemical Cycles* **21**,  
941 doi:10.1029/2006GB002788 (2007).

942 Sarma, V. V. S. S. *et al.* Sources and sinks of CO<sub>2</sub> in the west coast of Bay of Bengal. *Tellus*  
943 *B* **64**, 10961, doi:10.3402/tellusb.v64i0.10961 (2012).

944 Sarmiento, J. L., Gruber, N. *Ocean biogeochemical dynamics*. (Cambridge University Press,  
945 2006).

946 Sasse, T.P., McNeil, B.I., Abramowitz, G. A novel method for diagnosing seasonal to inter-annual  
947 surface ocean carbon dynamics from bottle data using neural networks. *Biogeosciences* **10**,  
948 4319 (2013).

949 Smith, S. V., Key, G. S. Carbon dioxide and metabolism in marine environments. *Limnol.*  
950 *Oceanogr* **20**, 493-495 (1975).

951 Takahashi, T. *et al.* Climatological mean and decadal change in surface ocean pCO<sub>2</sub>, and net  
952 sea-air CO<sub>2</sub> flux over the global oceans. *Deep-Sea Res. Pt II* **56**, 554-577,  
953 doi:10.1016/j.dsr2.2008.12.009 (2009).

954 Takahashi, T., Sutherland, S. Climatological mean distribution of pH and carbonate ion  
955 concentration in Global Ocean surface waters in the Unified pH scale and mean rate  
956 of their changes in selected areas. Report No. OCE 10-38891, (National Science  
957 Foundation, Washington, D. C., USA, 2013).

958 Taylor, An introduction to Error Analysis The study of uncertainties in physical  
959 measurements, *University Science Books*, second edition, 1997.

960 Ternon, J. F., Oudot, C., Dessier, A., Diverres, D. A seasonal tropical sink for atmospheric  
961 CO<sub>2</sub> in the Atlantic ocean: the role of the Amazon River discharge. *Marine Chemistry*  
962 **68**, 183-201, doi:http://dx.doi.org/10.1016/S0304-4203(99)00077-8 (2000).

963 Yang, D., Liu, Y., Cai, Z., Chen, X., Yao, L., Lu, D. First Global Carbon Dioxide Maps  
964 Produced from TanSat Measurements, *Advances in Atmospheric Sciences*, doi:  
965 10.1007/s00376-018-7312-6 (2018).

## Supporting Information for

### **Optimum satellite remote sensing of the marine carbonate system using empirical algorithms in the Global Ocean, the Greater Caribbean, the Amazon Plume and the Bay of Bengal**

Peter E. Land<sup>1</sup>, Helen S. Findlay<sup>1</sup>, Jamie D. Shutler<sup>2</sup>, Ian G.C. Ashton<sup>2</sup>, Thomas Holding<sup>2</sup>, Antoine Grouazel<sup>3</sup>, Fanny Girard-Adhuin<sup>3</sup>, Nicolas Reul<sup>3</sup>, Jean-Francois Piolle<sup>3</sup>, Bertrand Chapron<sup>3</sup>, Yves Quilfen<sup>3</sup>, Richard G.J. Bellerby<sup>4,5</sup>, Punyasloke Bhadury<sup>6</sup>, Joseph Salisbury<sup>7</sup>, Douglas Vandemark<sup>7</sup>, Roberto Sabia<sup>8</sup>

<sup>1</sup>Plymouth Marine Laboratory, Prospect Place, West Hoe, Plymouth, PL1 3DH, UK, <sup>2</sup>University of Exeter, Penryn, Cornwall, TR10 9FE, UK, <sup>3</sup>Ifremer, University Brest, CNRS, IRD, Laboratoire d'Océanographie Physique et Spatiale (LOPS), IUEM, F-29280, Brest, France, <sup>4</sup>SKLEC-NIVA Centre for Marine and Coastal Research, State Key Laboratory for Estuarine and Coastal Research, East China Normal University Zhongshan N. Road, 3663, Shanghai 200062, China, <sup>5</sup>Norwegian Institute for Water Research, Thormøhlensgate 53D, N-5006, Bergen, Norway, <sup>6</sup>Department of Biological Sciences, Indian Institute of Science Education and Research Kolkata, Mohanpur 741 246, West Bengal, India, <sup>7</sup>Ocean Processes Analysis Laboratory, University of New Hampshire, Durham, New Hampshire, 3824, United States, <sup>8</sup>Telespazio-Vega U.K. European Space Agency (ESA), ESRIN, Frascati, Italy

#### **Contents of this file**

Text S1 and S2  
Figure S1  
Datasets S1 to S23  
References

#### **Introduction**

Supporting information is provided on the details of the algorithms used in the analyses (Text S1) along with the input data nomenclature for the datasets (Text S2). The datasets themselves are provided in three versions within (Land et al., 2019) which is available at <https://doi.pangaea.de/10.1594/PANGAEA.898115>: the first uses all data; the second excludes grid cells containing areas with depth less than 500 m, and the third is the same as the second, but also excludes grid cells containing areas closer than 300 km to any coast. The matchup data used and outputs at each matchup are provided in Datasets S1 to S5 (.csv files). Summary statistics for each output are provided in Datasets S6 to S10 (.csv files). Data pertaining to the method of scoring outputs are provided in Datasets S11 to S15 (netCDF files). Maps of *in situ* and output data and their differences are provided in Datasets S16 to S20 (netCDF files). The effects of excluding algorithms and/or data sources are shown in Datasets S21 (all combinations) and S22 (selected combinations) (.csv files). Results of the comparison of total alkalinity ( $A_T$ ) and dissolved inorganic carbon ( $C_T$ ) retrievals are provided in Dataset S23 (.csv file).

## Text S1. Algorithm details.

(Lee et al. 2006)  $A_T$  algorithms (L06):

Regionally variable slope and intercept parameters (see (Lee et al. 2006) for details) for the following algorithm:

$$A_T = a + b(SSS - S) + c(SSS - S)^2 - d(SST - T) + e(SST - T)^2,$$

where  $S$  and  $T$  are salinity and temperature variables with fixed values for a given region.

Temperature and salinity ranges of validity in each region are specified in LeeEtAl2006.nc, included with the software.

(Takahashi and Sutherland 2013)  $A_T$  algorithms (TS13):

Regionally variable slope and intercept parameters (See (Takahashi and Sutherland 2013) for details) for the following algorithm:

$$A_T = (A_0 \times SSS + A_1) - NO_3$$

Note that there is a misprint in Table 1 of (Takahashi and Sutherland 2013) – the intercept of Region 25 Antarctic (Pacific) should read -450.8 rather than 450.8, as shown in Figure 6 of (Takahashi and Sutherland 2013).

Salinity ranges of validity in each region are specified in TakahashiSutherland.nc, included with the software.

(Sasse et al. 2013)  $A_T$  algorithms (S13 and S13g):

Regionally variable plus global slope and intercept parameters (See (Sasse et al. 2013) for details) for the following algorithm:

$$A_T = a + bSST + cSSS + dSSS^2 + eDO + fSi + gPO_4 + \text{interaction terms.}$$

We found no information in (Sasse et al. 2013) about data ranges, so these algorithms are applied to all data.

(Cai et al. 2010) and (Lefèvre et al. 2010)  $A_T$  algorithms:

Simple linear relationships of  $A_T$  with  $SSS$  for the Greater Caribbean (Cai et al. 2010 only) and Amazon Plume regions (see (Cai et al. 2010; Lefèvre et al. 2010) for details).

The salinity range of applicability of (Cai et al. 2010) is 32.9 to 37.8 in the Greater Caribbean and 23.8 to 38.1 in the Amazon Plume, and that of (Lefèvre et al. 2010) is 17 to 37.

(Lee et al. 2000)  $C_T$  algorithms (L00):

Regionally variable slope and intercept parameters (See (Lee et al. 2000) for details) for the following algorithm:

$$nC_T = a + b \times SST + c \times SST^2 + d \times NO_3$$

$$nC_T = C_T \times \frac{35}{SSS}$$

Between 30°N and 30°S, (Lee et al. 2000) increase  $nC_T$  by 1  $\mu\text{mol kg}^{-1}$  per year.

Temperature and salinity ranges of validity in each region are specified in LeeEtAl2000.nc, included with the software.



(Sasse et al. 2013)  $C_T$  algorithms (S13 and S13g):

Regionally variable plus global slope and intercept parameters (See (Sasse et al. 2013) for details) for the following algorithm:

$$C_T = a + bSST + cSSS + dDO^2 + eNO_3 + fSi + gPO_4 + \text{interaction terms.}$$

(Sasse et al. 2013) include a calculated correction for the anthropogenic increase in  $C_T$  with a global average of  $1 \text{ umol kg}^{-1}$  per year. Here we use the global average value for simplicity and consistency with (Lee et al. 2000).

We found no information in (Sasse et al. 2013) about data ranges, so these algorithms are applied to all data.

(Lefèvre et al. 2010) and (Bonou et al. 2016)  $C_T$  algorithms:

Simple linear relationships of  $C_T$  with SSS for the Amazon Plume Region (see (Bonou et al. 2016; Lefèvre et al. 2010) for details). (Bonou et al. 2016) increase  $C_T$  by  $0.9 \text{ umol kg}^{-1}$  per year.

The salinity range of applicability of (Lefèvre et al. 2010) is 17 to 37, and that of (Bonou et al. 2016) is 0 to 38.3.

**Text S2: Details of the input parameter nomenclature**

Parameter names ending in “\_CLIM” are monthly climatologies, i.e. 12 climatologies for January to December. All other names indicate multi-year monthly data. So an *in situ* measurement from January 2010 would be compared with the January part of \_CLIM datasets, and the January 2010 part of all other datasets.

HG2 and HG2\_CLIM:

The Met Office Hadley Centre, Hadley Global Environment Model 2 - Earth System (HadGEM2-ES) multi-year monthly dataset and monthly climatology.

SSS\_WOA\_CLIM, SST\_WOA\_CLIM, DO\_WOA\_CLIM, NITRATE\_WOA\_CLIM, SILICATE\_WOA\_CLIM and PHOSPHATE\_WOA\_CLIM:

World Ocean Atlas 2013 (WOA) monthly climatologies, spatially interpolated to 1°×1° (Garcia et al. 2014a; Garcia et al. 2014b; Locarnini et al. 2013; Zweng et al. 2013). Note that WOA nitrate is actually nitrate + nitrite.

SSS\_SMOS and SSS\_SMOS\_CLIM:

SMOS satellite SSS multi-year monthly datasets and monthly climatology.

SSS\_AQUARIUS and SSS\_AQUARIUS\_CLIM:

Aquarius satellite SSS multi-year monthly datasets and monthly climatology.

SSS\_CORA, SSS\_CORA\_CLIM, SST\_CORA and SST\_CORA\_CLIM:

Coriolis Ocean ReAnalysis database (version 4.0), which includes data from ARGO, the global network of moored buoys (including TAO/TRITON, PIRATA, RAMA buoys), underwater gliders (EGO), GTSP, Ships of opportunity, sea mammals equipped with sensors, and other integrated datasets from CTDs, oceanographic cruises, etc. This database is output in two sets: \_CORACLIM is the monthly climatology; and \_CORA is the multi-year monthly dataset.

SST\_CCI and SST\_CCI\_CLIM:

Sea Surface Temperature Climate Change Initiative data archives from ESA’s ATSR and AATSR.

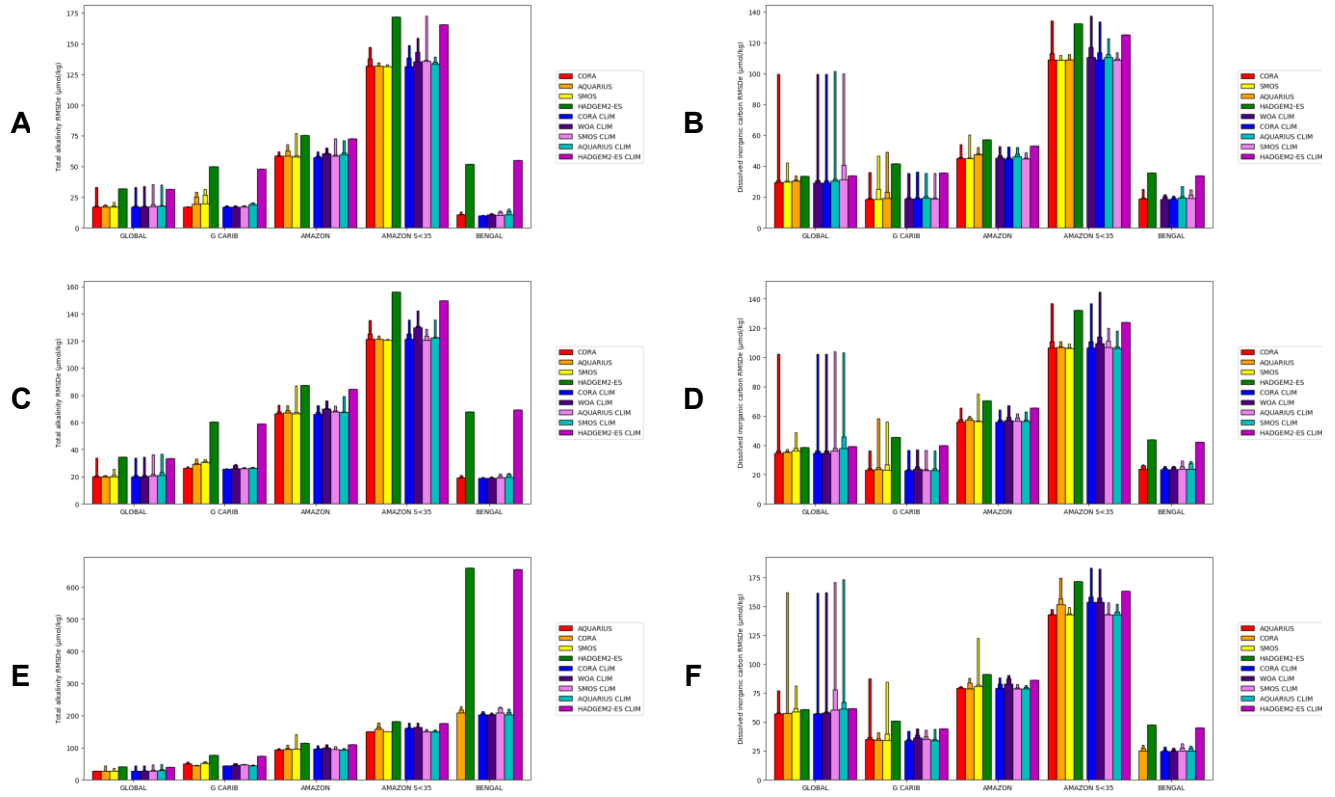


Figure S1: Equivalent plots to that of Figure 1 in the main manuscript but with alternative depth and coastal masking. (A) repeat of Figure 1(A),  $A_T$  with minimum depth 500 m and minimum distance to coast 300 km masked; (B) repeat of Figure 1(B),  $C_T$  with minimum depth 500 m and minimum distance to coast 300 km masked; (C)  $A_T$  with minimum depth 500 m; (D)  $C_T$  with minimum depth 500 m; (E)  $A_T$  with no masking; (F)  $C_T$  with no masking.

## Datasets introduction

In the following datasets, which are all available within Land et al., (2019). 'X' denotes one of three versions: " corresponds to all data, 'Depth500' to a minimum depth of 500 m, and 'Depth500Dist300' to a minimum depth of 500 m and a minimum distance to coast of 300 km. Each of the three versions is contained in its own directory.

**Datasets S1 to S5** are .csv files containing all matchups in each region, including date and location, *in situ*  $A_T$  and  $C_T$  measurements and estimated uncertainties, all input datasets, estimates of  $A_T$  and  $C_T$  from all outputs, and the best available output estimates of  $A_T$  and  $C_T$  for each matchup (see main text).

S1\_GlobalAlgorithmMatchupsX.csv  
S2\_GreaterCaribbeanAlgorithmMatchupsX.csv  
S3\_AmazonPlumeAlgorithmMatchupsX.csv  
S4\_AmazonPlumeLowSAAlgorithmMatchupsX.csv  
S5\_BayOfBengalAlgorithmMatchupsX.csv

**Datasets S6 to S10** are .csv files containing statistics of all outputs in each region, including the carbonate system variable, algorithm, input datasets used, (MAD, RMSD using all available data, output score, RMSD estimated from output score, output and *in situ* mean and standard deviation, correlation coefficient), all items in brackets presented both unweighted and weighted, number of matchups, number of potential matchups, matchup coverage, RMSD after subtraction of linear regression, percentage reduction in RMSD due to subtraction of linear regression and weighted score divided by number of matchups (see main text for explanation of terms).

S6\_GlobalAlgorithmScoresX.csv  
S7\_GreaterCaribbeanAlgorithmScoresX.csv  
S8\_AmazonPlumeAlgorithmScoresX.csv  
S9\_AmazonPlumeLowSAAlgorithmScoresX.csv  
S10\_BayOfBengalAlgorithmScoresX.csv

**Datasets S11 to S15** are netCDF files containing error analyses of all outputs in each region, including the squared error of each output at each matchup, the weight of each squared error (1/squared uncertainty), weight \* squared error, number of matchups available to each output, number of matchups available to each combination of two outputs, (score of each output in a given comparison of two outputs, overall output score and RMSD estimated from output score), all items in the last brackets presented both unweighted and weighted.

S11\_GlobalSquaredErrorsX.nc  
S12\_GreaterCaribbeanSquaredErrorsX.nc  
S13\_AmazonPlumeSquaredErrorsX.nc  
S14\_AmazonPlumeLowSSquaredErrorsX.nc  
S15\_BayOfBengalSquaredErrorsX.nc

**Datasets S16 to S20** are netCDF files containing global maps of the data in Tables S4 to S9, showing the spatial distribution of the mean and standard deviation of each of: *in situ* data; output data; output data – *in situ* data and number of matchups. Regional files show the same maps, but only including data within the region.

S16\_GlobalmapsX.nc  
S17\_GreaterCaribbeanmapsX.nc  
S18\_AmazonPlumemapsX.nc

S19\_AmazonPlumeLowSmapsX.nc  
S20\_BayOfBengalmapsX.nc

**Datasets S21 and S22** are .csv files containing the effect on estimated RMSD of excluding various combinations of algorithms and/or inputs for  $A_T$  and  $C_T$  in each region. For a given variable and region, the first line shows the algorithm, input data sources, estimated RMSD and bias of the output with lowest estimated RMSD. Subsequent lines show the effect of excluding combinations of algorithms and/or inputs, ordered first by the number of algorithms/inputs excluded (fewest first), then by effect on lowest estimated RMSD. So the first line(s) consist of the effects of excluding the best algorithm and each of the input sources to that algorithm, most important first. Each line consists of the item excluded, ratio of resulting estimated RMSD to original estimated RMSD, resulting bias and number of items excluded. Some exclusions are equivalent, for instance exclusion of WOA nitrate (the only nitrate source) is equivalent to excluding all algorithms using nitrate. Dataset S21 contains a comprehensive list of all possible exclusions, and so is rather hard to read and interpret. To mitigate this, Dataset S22 contains only those exclusion sets with effect greater than 1% and at least 0.1% greater than any subset of its exclusions.

S21\_importancesX.csv  
S22\_importances2X.csv

**Dataset S23** is a .csv file containing like-for-like comparisons of RMSD between  $A_T$  and  $C_T$  in each region. Bear in mind that the RMSD shown here is not the same as the estimated RMSD (RMSDe in the main text) shown elsewhere.

S23\_TA\_DICcomparisonX.csv

## References

- Bonou, F.K., Noriega, C., Lefèvre, N., & Araujo, M. (2016). Distribution of CO<sub>2</sub> parameters in the Western Tropical Atlantic Ocean. *Dynamics of Atmospheres and Oceans*, 73, 47-60
- Cabanes, C., Grouazel, A., Schuckmann, K.v., Hamon, M., Turpin, V., Coatanoan, C., Paris, F., Guinehut, S., Boone, C., & Ferry, N. (2013). The CORA dataset: validation and diagnostics of in-situ ocean temperature and salinity measurements. *Ocean Science*, 9, 1-18
- Cai, W.-J., Hu, X., Huang, W.-J., Jiang, L.-Q., Wang, Y., Peng, T.-H., & Zhang, X. (2010). Alkalinity distribution in the western North Atlantic Ocean margins. *Journal of Geophysical Research: Oceans*, 115, n/a-n/a
- Choudhury, A.K., Das, M., Philip, P., & Bhadury, P. (2015). An assessment of the implications of seasonal precipitation and anthropogenic influences on a mangrove ecosystem using phytoplankton as proxies. *Estuaries and Coasts*, 38, 854-872
- Findlay, H.S., Tyrrell, T., Bellerby, R.G.J., Merico, A., & Skjelvan, I. (2008). Carbon and nutrient mixed layer dynamics in the Norwegian Sea. *Biogeosciences*, 5, 1395-1410
- Garcia, H.E., Locarnini, R.A., Boyer, T.P., Antonov, J.I., Baranova, O.K., Zweng, M.M., Reagan, J.R., & Johnson, D.R. (2014a). World ocean atlas 2013. Volume 3, Dissolved oxygen, apparent oxygen utilization, and oxygen saturation, edited by: Levitus, S. *A. Mishonov Technical Ed., NOAA Atlas NESDIS*, 75, 27

Garcia, H.E., Locarnini, R.A., Boyer, T.P., Antonov, J.I., Baranova, O.K., Zweng, M.M., Reagan, J.R., Johnson, D.R., Mishonov, A.V., & Levitus, S. (2014b). World ocean atlas 2013. Volume 4, Dissolved inorganic nutrients (phosphate, nitrate, silicate), edited by: Levitus, S. *A. Mishonov Technical Ed., NOAA Atlas NESDIS, 76, 25*

Jones, C.D., Hughes, J.K., Bellouin, N., Hardiman, S.C., Jones, G.S., Knight, J., Liddicoat, S., O'Connor, F.M., Andres, R.J., Bell, C., Boo, K.O., Bozzo, A., Butchart, N., Cadule, P., Corbin, K.D., Doutriaux-Boucher, M., Friedlingstein, P., Gornall, J., Gray, L., Halloran, P.R., Hurtt, G., Ingram, W.J., Lamarque, J.F., Law, R.M., Meinshausen, M., Osprey, S., Palin, E.J., Parsons Chini, L., Raddatz, T., Sanderson, M.G., Sellar, A.A., Schurer, A., Valdes, P., Wood, N., Woodward, S., Yoshioka, M., & Zerroukat, M. (2011). The HadGEM2-ES implementation of CMIP5 centennial simulations. *Geoscientific Model Development, 4, 543-570*

Land, P. E., Findlay, H. S., Shutler, J. D., Ashton, I. G. C., Grouazel, A., Girard-Ardhuin, F., Reul, N., Piolle, J. –F., Chapron, B., Quilfen, Y., Bellerby, R. G. J., Bhadury, P., Salisbury, J., Vandemark, D., Sabia, R., (2019) Results and analysis of oceanic total alkalinity and dissolved inorganic carbon estimated from space borne, interpolated in situ, climatological and Earth system model data. *PANGAEA*, doi:10.1594/PANGAEA.898115.

Le Vine, D.M., Dinnat, E.P., Lagerloef, G.S.E., Matthaeis, P., Abraham, S., Utku, C., & Kao, H. (2014). Aquarius: Status and recent results. *Radio Science, 49, 709-720*

Lee, K., Tong, L.T., Millero, F.J., Sabine, C.L., Dickson, A.G., Goyet, C., Park, G.H., Wanninkhof, R., Feely, R.A., & Key, R.M. (2006). Global relationships of total alkalinity with salinity and temperature in surface waters of the world's oceans. *Geophysical Research Letters, 33*

Lee, K., Wanninkhof, R., Feely, R.A., Millero, F.J., & Peng, T.H. (2000). Global relationships of total inorganic carbon with temperature and nitrate in surface seawater. *Global Biogeochemical Cycles, 14, 979-994*

Lefèvre, N., Diverrès, D., & Gallois, F. (2010). Origin of CO<sub>2</sub> undersaturation in the western tropical Atlantic. *Tellus B, 62, 595-607*

Locarnini, R.A., Mishonov, A.V., Antonov, J.I., Boyer, T.P., Garcia, H.E., Baranova, O.K., Zweng, M.M., Paver, C.R., Reagan, J.R., Johnson, D.R., Hamilton, M., & Seidov, D. (2013). World Ocean Atlas 2013, Volume 1: Temperature, edited by: Levitus, S. *A. Mishonov Technical Ed., NOAA Atlas NESDIS, 73, 40*

Merchant, C.J., Embury, O., Rayner, N.A., Berry, D.I., Corlett, G.K., Lean, K., Veal, K.L., Kent, E.C., Llewellyn-Jones, D.T., & Remedios, J.J. (2012). A 20 year independent record of sea surface temperature for climate from Along-Track Scanning Radiometers. *Journal of Geophysical Research: Oceans (1978–2012), 117*

Olsen, A., Key, R.M., van Heuven, S., Lauvset, S.K., Velo, A., Lin, X., Schirnick, C., Kozyr, A., Tanhua, T., Hoppema, M., Jutterström, S., Steinfeldt, R., Jeansson, E., Ishii, M., Pérez, F.F., & Suzuki, T. (2016). The Global Ocean Data Analysis Project version 2 (GLODAPv2) – an internally consistent data product for the world ocean. *Earth System Science Data, 8, 297-323*

Reul, N., & Team, I.C.-C. (2011). SMOS L3 SSS Research Products: Product User Manual Reprocessed Year 2010. In. IFREMER, Plouzané, France

Sasse, T.P., McNeil, B.I., & Abramowitz, G. (2013). A novel method for diagnosing seasonal to inter-annual surface ocean carbon dynamics from bottle data using neural networks. *Biogeosciences*, 10, 4319

Takahashi, T., & Sutherland, S. (2013). Climatological mean distribution of pH and carbonate ion concentration in Global Ocean surface waters in the Unified pH scale and mean rate of their changes in selected areas. In. Washington, D. C., USA: National Science Foundation

Takahashi, T., Sutherland, S.C., & Kozyr, A. (2013). Global Ocean Surface Water Partial Pressure of CO<sub>2</sub> Database: Measurements Performed During 1957-2012 (Version 2012). In. Oak Ridge, Tennessee, USA: Carbon Dioxide Information Analysis Center, Oak Ridge National Laboratory, U.S. Department of Energy

Zweng, M.M., Reagan, J.R., Antonov, J.I., Locarnini, R.A., Mishonov, A.V., Boyer, T.P., Garcia, H.E., Baranova, O.K., Johnson, D.R., & Seidov, D. (2013). World ocean atlas 2013. Volume 2, Salinity. *A. Mishonov Technical Ed., NOAA Atlas NESDIS, 74*, 39